Bull Math Biol (2016) 78:2304–2357
DOI 10.1007/s11538-016-0179-8

ORIGINAL ARTICLE

A Mathematical Model of Granulopoiesis Incorporating the Negative Feedback Dynamics and Kinetics of G-CSF/Neutrophil Binding and Internalization

M. Craig[1,2] · **A. R. Humphries**[3] · **M. C. Mackey**[4]

Received: 21 December 2015 / Accepted: 19 May 2016 / Published online: 20 June 2016

Abstract We develop a physiological model of granulopoiesis which includes explicit modelling of the kinetics of the cytokine granulocyte colony-stimulating factor (G-CSF) incorporating both the freely circulating concentration and the concentration of the cytokine bound to mature neutrophils. G-CSF concentrations are used to directly regulate neutrophil production, with the rate of differentiation of stem cells to neutrophil precursors, the effective proliferation rate in mitosis, the maturation time, and the release rate from the mature marrow reservoir into circulation all dependent on the level of G-CSF in the system. The dependence of the maturation time on the cytokine concentration introduces a state-dependent delay into our differential equation model, and we show how this is derived from an age-structured partial differential equation model of the mitosis and maturation and also detail the derivation of the rest of our model. The model and its estimated parameters are shown to successfully predict the neutrophil and G-CSF responses to a variety of treatment scenarios, including the combined administration of chemotherapy and exogenous G-CSF. This concomitant

✉ M. Craig
morgan.craig@umontreal.ca

A. R. Humphries
tony.humphries@mcgill.ca

M. C. Mackey
michael.mackey@mcgill.ca

1 Faculté de Pharmacie, Université de Montréal, Montréal, QC H3T 1J4, Canada

2 Present Address: Program for Evolutionary Dynamics, Harvard University, Cambridge, MA 02138, USA

3 Department of Mathematics and Statistics, McGill University, Montréal, QC H3A 0B9, Canada

4 Departments of Mathematics, Physics and Physiology, McGill University, Montréal, QC H3G 1Y6, Canada

treatment was reproduced *without any additional fitting* to characterize drug–drug interactions.

Keywords Granulopoiesis · Mathematical modelling · State-dependent delay differential equations · Physiologically constructed pharmacokinetics · G-CSF · Bound and unbound drug concentrations

1 Introduction

We present a new model of granulopoiesis, in which the production of neutrophils is governed by a negative feedback loop between the neutrophils and granulocyte colony-stimulating factor (G-CSF). G-CSF is the principal cytokine known to regulate neutrophil production and in our model it is used to moderate differentiation of stem cells, apoptosis of proliferating neutrophil precursors, the speed at which neutrophils mature, and the rate that mature neutrophils are released from the marrow reservoir. To facilitate this, we derive not only new functions for the pharmacodynamic effects of G-CSF, but also a new model of the G-CSF kinetics which incorporates cytokine binding and internalization by the neutrophils. We dispense with the mass action law assumption made in some previous models and directly model the concentration of both circulating G-CSF and G-CSF bound to neutrophils. This improved kinetic model furnishes us with G-CSF concentrations which are considerably more accurate than our previous models so we are able to use them to directly drive the pharmacodynamic effects and finally form a fully closed cytokine-neutrophil feedback loop.

At homeostasis the dominant removal mechanism for G-CSF is internalization by neutrophils after it binds to receptors on these cells (Layton and Hall 2006). This gives rise to a negative feedback mechanism on the G-CSF pharmacokinetics (PKs) whereby large concentrations of neutrophils result in G-CSF being removed from circulation, in turn leading to low concentrations of circulating G-CSF. On the other hand if neutrophil concentrations are reduced then G-CSF is not cleared from circulation as quickly and circulating concentrations increase as a result. The feedback loop is completed by the pharmacodynamic (PD) effects of the G-CSF: Elevated (depressed) G-CSF levels lead to increased (decreased) neutrophil production. Due to this feedback, using the simple paradigm that neutrophil concentration is a cipher for the cytokine concentration (with one low when the other is high), it is possible to derive granulopoiesis models without explicitly modelling the cytokines. This can be useful because it is not universally agreed where or how the multitude of identified cytokines all act.

The mathematical modelling of granulopoiesis has a long and rich history (Bernard et al. 2003; Brooks et al. 2012; Colijn and Mackey 2005b; Craig et al. 2015; Foley et al. 2006; Foley and Mackey 2009b; Hearn et al. 1998; Kazarinoff and Driessche 1979; King-Smith and Morley 1970; Schirm et al. 1996; Schmitz 1988; Schmitz et al. 1990; Scholz et al. 2005; Shvitra et al. 1983; Wichmann and Loffler 1988; Vainas et al. 2012; Vainstein et al. 2005; von Schulthess and Mazer 1982), but one of the earliest and most complete treatments is that of Rubinow and Lebowitz (1975) which incorporates a number of features that we retain in our model, including active proliferation, maturation, a marrow reservoir, and free exchange between the circulating and mar-

ginal blood neutrophil pools. Rubinow's model, however, predates the discovery and characterization of G-CSF and so it uses neutrophil concentrations as a cipher for the cytokine and its effects. Subsequent physiological models have also all incorporated at least some elements of this cytokine paradigm in their modelling. Some authors have been principally interested in neutrophil pathologies, including cyclical neutropenia, chronic myeloid leukemia, and myelosuppression during chemotherapy, while others have primarily studied the effects of G-CSF mimetics. Many models of cyclic neutropenia, including Colijn and Mackey (2005b), Foley et al. (2006), Hearn et al. (1998), Lei and Mackey (2011), and Schmitz et al. (2014), acknowledge the role of G-CSF in neutrophil production and pathologies but rely on the cytokine paradigm to drive the pharmacodynamic responses. A number of different modelling approaches have been proposed, including compartmental ODE models (Schirm et al. 1996; Friberg and Karlsson 2003; Quartino et al. 2012; González-Sales et al. 2012; Krzyzanski et al. 2010; Wang et al. 2001), delay differential equations (DDEs) incorporating statistical distributions to model delays (Vainstein et al. 2005; Vainas et al. 2012) and DDEs derived from age-structured partial differential equation (PDE) models, like the one developed in this work (Brooks et al. 2012; Craig et al. 2015; Foley and Mackey 2009b).

In recent years, synthetic forms of G-CSF have been developed and are administered to patients for a variety of reasons, including to treat cyclical neutropenia or as an adjuvant during chemotherapy (Dale and Mackey 2015; Dale and Welte 2011; Molineux et al. 2012). However, the administration of exogenous G-CSF breaks the cytokine paradigm and it is possible for neutrophil and G-CSF concentrations to both be elevated at the same time. This breakdown of the natural feedback relationship can cause physiological models that use the paradigm to mischaracterize the elimination dynamics of G-CSF. For example, both Krzyzanski et al. (2010) and Craig et al. (2015) overestimate the renal clearance of G-CSF so much as to essentially eliminate the contribution of neutrophil-mediated internalization, even though they each include this nonlinear clearance in their models. If elevated neutrophil concentrations are used to drive the system dynamics on the assumption that corresponding G-CSF concentrations are reduced when they are in fact elevated, the modelled effects will act in the opposite sense to the physiology. As a consequence, the model will either develop instabilities and/or give a poor fit to observed dynamics.

The mischaracterization of G-CSF elimination dynamics was the impetus for the current work. Consequently, we will not use the neutrophil concentration as a cipher for the G-CSF concentration, but will model both the G-CSF pharmacokinetics and pharmacodynamics (PK/PD) in detail. For this, we develop a novel pharmacokinetic model of G-CSF which includes both unbound and bound blood concentrations. The G-CSF concentrations given by this kinetic model are then used to drive the pharmacodynamic effects of the cytokine, in a fully formed negative feedback loop.

We begin by summarizing the granulopoiesis model in Sect. 2. Its development is then extensively detailed in Sect. 3, beginning from the stem cells in Sect. 3.1. The novel pharmacokinetic G-CSF model incorporating bound and unbound blood concentrations is motivated and developed in Sect. 3.2. There we show how the hypothesis of an equilibrium between bound and unbound concentrations is not satisfied for G-CSF, necessitating the inclusion of more complex kinetics in its pharmacokinetic model.

Next, the derivation of the DDE granulopoiesis model is given in Sect. 3.3 and the pharmacodynamic model of G-CSF is developed in Sect. 3.4. Models of the exogenous drugs considered in our study are detailed in Sect. 3.5. Having laid the foundations of our model, the various methods of parameter estimation and fitting used for our analyses are subsequently explained in Sect. 4. These approaches include model-specific constraints, as seen in Sects. 4.1 and 4.3, while fitting procedures from published data are described in Sects. 4.2, 4.4, and 4.5. The resulting parameters are then summarized in Sect. 5. Finally in Sect. 6 we put our model to the acid test of *predicting (not fitting)* the population neutrophil response in a group of patients undergoing simultaneous chemotherapy and G-CSF administration (Pfreundschuh et al. 2004a, b) and obtain excellent agreement between the model predicted behavior and the clinical data. We conclude with a short discussion in Sect. 7.

2 Model Summary

Here we define the variables and summarize the equations that define our granulopoiesis model. A detailed derivation is contained in Sect. 3. Figure 1 shows a schematic diagram describing the main elements of the hematopoietic system that we model.

The hematopoietic stem cell (HSC), neutrophil, and G-CSF model is a set of five differential equations including constant and state-dependent delays. Let $Q(t)$ be the concentration of HSCs at time t, $N_R(t)$ be the concentration of mature neutrophils in the marrow reservoir, and $N(t)$ be the concentration of the total blood neutrophil pool (TBNP) at time t (which includes both circulating and marginated neutrophils). Further, let $G_1(t)$ be the concentration of unbound, circulating G-CSF and $G_2(t)$ be the concentration of G-CSF bound to receptors on mature neutrophils (in the reservoir or in the blood neutrophil pool).

The production of neutrophils from the HSCs is modelled by

$$\begin{aligned}\frac{\mathrm{d}}{\mathrm{d}t}Q(t) &= -\big(\kappa(G_1(t)) + \kappa_\delta + \beta(Q(t))\big)Q(t)\\ &\quad + A_Q(t)\beta\left(Q(t-\tau_Q)\right)Q(t-\tau_Q) \qquad (1)\\ \frac{\mathrm{d}}{\mathrm{d}t}N_R(t) &= A_N(t)\kappa(G_1(t-\tau_N(t)))Q(t-\tau_N(t))\frac{V_{N_M}(G_1(t))}{V_{N_M}(G_1(t-\tau_{N_M}(t)))}\\ &\quad -\big(\gamma_{N_R} + \varphi_{N_R}(G_{BF}(t))\big)N_R(t) \qquad (2)\\ \frac{\mathrm{d}}{\mathrm{d}t}N(t) &= \varphi_{N_R}(G_{BF}(t))N_R(t) - \gamma_N N(t), \qquad (3)\end{aligned}$$

with the concentrations of G-CSF (unbound and bound to neutrophil G-CSF receptors) given by

$$\begin{aligned}\frac{\mathrm{d}}{\mathrm{d}t}G_1(t) &= I_G(t) + G_{\mathrm{prod}} - k_{\mathrm{ren}}G_1(t)\\ &\quad - k_{12}([N_R(t)+N(t)]V - G_2(t))G_1(t)^{\mathrm{Pow}} + k_{21}G_2(t) \qquad (4)\\ \frac{\mathrm{d}}{\mathrm{d}t}G_2(t) &= -k_{\mathrm{int}}G_2(t) + k_{12}\big([N_R(t)+N(t)]V - G_2(t)\big)G_1(t)^{\mathrm{Pow}} - k_{21}G_2(t), \qquad (5)\end{aligned}$$

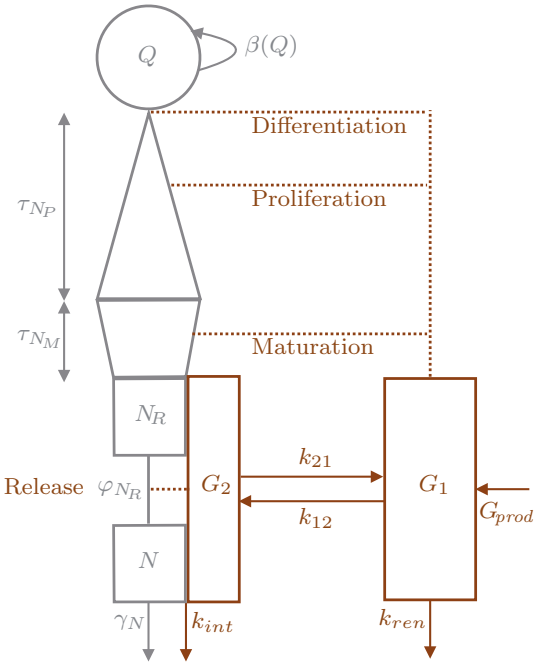

Fig. 1 Schematic representation of the production of circulating neutrophils in the bone marrow and the interaction of the system with G-CSF. Hematopoietic stem cells (HSCs-Q) enter the neutrophil lineage, the other blood lines, or are removed from the HSC pool. Differentiated HSCs undergo successive divisions during the proliferative phase. Cells then mature before being stored in the marrow reservoir, or dying off during maturation. Neutrophils remain in the reservoir until they are removed randomly or enter the circulation, where they disappear rapidly from the blood. Freely circulating G-CSF may bind to receptors on the neutrophils. The concentration of bound G-CSF drives its pharmacodynamic effects. The concentration of G-CSF bound to mature neutrophils, G_2, determines the rate of release from the marrow reservoir. The concentration of G-CSF bound to neutrophil precursors, assumed proportional to G_1 the concentration of freely circulating G-CSF, determines the rate of differentiation from the HSCs, the speed of maturation, and the rate of proliferation. For all four effects, speed and rates increase with increasing G-CSF concentration

where $I_G(t)$ indicates input of exogenous G-CSF, which we assume is filgrastim (the most common biosimilar exogenous form of G-CSF). Filgrastim has very similar PK/PD properties to endogenous G-CSF, so we will not distinguish between the two types of G-CSF in our model.

The derivation of these equations is given in Sect. 3. In Sect. 3.3, particular attention is paid to the derivation of the state-dependent delay terms in (2) from an age-structured partial differential equation (PDE) model of the mitosis and maturation with variable aging rate of the neutrophil precursors. The G-CSF Eqs. (4), (5) are explained in detail in Sect. 3.2.

In the stem cell Eq. (1), as explained in Sect. 3.1, we have

$$\beta(Q) = f_Q \frac{\theta_2^{s_2}}{\theta_2^{s_2} + Q^{s_2}}, \tag{6}$$

$$A_Q(t) = A_Q^* = 2e^{-\gamma_Q \tau_Q}. \tag{7}$$

Only in the case of administration of chemotherapy is the stem cell amplification factor $A_Q(t)$ nonconstant. During chemotherapeutic treatment $A_Q(t)$ will be modified by replacing (7) with (38) as discussed in Sect. 3.5. Stem cells commit to differentiate to neutrophil precursors at a rate given by

$$\kappa(G_1) = \kappa^* + \left(\kappa^* - \kappa^{\min}\right)\left[\frac{G_1^{s_1} - (G_1^*)^{s_1}}{G_1^{s_1} + (G_1^*)^{s_1}}\right]. \tag{8}$$

Here, and throughout, the superscript * denotes the homeostasis value of a quantity. The rationale for using (8) to describe the pharmacodynamic effect of the G-CSF on the differentiation of the HSCs along with the other G_1-dependent functions is explained in Sect. 3.4.

After entering the neutrophil lineage, cells undergo mitosis at a variable rate $(\eta_{N_P}(G_1(t)))$ given by

$$\eta_{N_P}(G_1(t)) = \eta_{N_P}^* + \left(\eta_{N_P}^* - \eta_{N_P}^{\min}\right)\frac{b_{N_P}}{G_1^*}\left(\frac{G_1(t) - G_1^*}{G_1(t) + b_{N_P}}\right) \tag{9}$$

for a proliferation time τ_{N_P}, considered to be constant. Cells subsequently mature at a variable aging rate given by

$$V_{N_M}(G_1(t)) = 1 + (V_{\max} - 1)\frac{G_1(t) - G_1^*}{G_1(t) - G_1^* + b_V}, \tag{10}$$

until they reach age a_{N_M} so the time $\tau_{N_M}(t)$ it takes for a neutrophil maturing at time t to mature satisfies the integral relationship

$$\int_{t-\tau_{N_M}(t)}^{t} V_{N_M}(G_1(s))ds = a_{N_M}. \tag{11}$$

At homeostasis, $V_{N_M}(G_1^*) = 1$, and thus, a_{N_M} is the homeostatic maturation time. The total time it takes a neutrophil to be produced (from HSC differentiation to release into the reservoir pool) is

$$\tau_N(t) = \tau_{N_P} + \tau_{N_M}(t), \tag{12}$$

and we can differentiate Eq. (11) to obtain the following DDE for both τ_N and τ_{N_M}

$$\frac{\mathrm{d}}{\mathrm{d}t}\tau_N(t) = \frac{\mathrm{d}}{\mathrm{d}t}\tau_{N_M}(t) = 1 - \frac{V_{N_M}(G_1(t))}{V_{N_M}(G_1(t - \tau_{N_M}(t)))}. \tag{13}$$

Maturing neutrophils are assumed to die at a constant rate given by γ_{N_M}. The amplification factor $A_N(t)$ between differentiation from HSCs to maturation that appears in (2) is then given by

$$A_N(t) = \exp\left[\int_{t-\tau_N(t)}^{t-\tau_{N_M}(t)} \eta_{N_P}(G_1(s))\mathrm{d}s - \gamma_{N_M}\tau_{N_M}(t)\right] \tag{14}$$

as derived in Sect. 3.3. Numerical implementation of the neutrophil amplification rate is obtained by differentiating the integral expressions in (14) using Leibniz's rule to obtain

$$\begin{aligned}\frac{\mathrm{d}}{\mathrm{d}t}A_N(t) = A_N(t)\Big[\big(1 - \frac{\mathrm{d}}{\mathrm{d}t}\tau_{N_M}(t)\big)\big(\eta_{N_P}(G_1(t-\tau_{N_M}(t))) - \eta_{N_P}(G_1(t-\tau_N(t)))\big) \\ - \gamma_{N_M}\frac{\mathrm{d}}{\mathrm{d}t}\tau_{N_M}(t)\Big].\end{aligned} \tag{15}$$

After maturation neutrophils are sequestered into the marrow neutrophil reservoir. Mature neutrophils exit the reservoir either by dying with constant rate γ_{N_R} or by being released into circulation with a rate φ_{N_R} depending on the fraction $G_{BF}(t)$ of neutrophil receptors that are bound by G-CSF. We define

$$G_{BF}(t) = \frac{G_2(t)}{V[N_R(t) + N(t)]} \in [0,1], \quad G^*_{BF} = \frac{G^*_2}{V[N^*_R + N^*]}, \tag{16}$$

and let

$$\varphi_{N_R}(G_{BF}(t)) = \varphi^*_{N_R} + \big(\varphi^{\max}_{N_R} - \varphi^*_{N_R}\big)\frac{G_{BF}(t) - G^*_{BF}}{G_{BF}(t) - G^*_{BF} + b_G}. \tag{17}$$

Neutrophils are removed from circulation with constant rate γ_N.

In Eqs. (1)–(5) we use units of 10^9 cells/kg (of body mass) for the reservoir and circulating neutrophils, and 10^6 cells/kg for the stem cells. The scaling factors ensure that computations are performed with numbers of similar magnitude which improves numerical stability. Circulating and bound G-CSF concentrations are measured in standard units of nanograms per milliliter of blood. The differing units for neutrophils and G-CSF are only problematical in Eqs. (4), (5) where quantities in both units appear; see Sect. 4.2 for the derivation of the conversion factor V.

Its also important to note that $N(t)$ measures the total blood neutrophil pool, including both the circulating and marginated neutrophils. To convert $N(t)$ to an absolute neutrophil count/circulating neutrophil numbers $N_C(t)$ (or *vice versa*) there is a conversion factor; see (93).

3 Model Development

Here we describe the development of our granulopoiesis model leading to the equations presented in Sect. 2. The equation for the stem cells (1) is described briefly in Sect. 3.1. The size of the mature neutrophil reservoir is described by (2). The first term on the right-hand side of this equation gives the rate that mature neutrophils enter the reservoir. This term is derived from an age-structured PDE model described in Sect. 3.3 below. In Sect. 3.2 we describe our new G-CSF model (4), (5) of the unbound freely circulating G-CSF (G_1), and the G-CSF bound to receptors on the neutrophils (G_2). This model allows us to model the pharmacodynamic effects of the G-CSF directly as detailed

in Sect. 3.4. Finally, Sect. 3.5 outlines our models for the exogenous drugs we will consider in later sections.

3.1 Stem Cells

Equation (1) for the HSC dynamics was previously used in Mackey (2001), Colijn and Mackey (2005a), Colijn and Mackey (2005b), Pujo-Menjouet et al. (2005), Foley and Mackey (2009b), Lei and Mackey (2011), Brooks et al. (2012), and Craig et al. (2015). In this model HSCs are generally quiescent, but may enter a mitotic phase at rate $\beta(Q)$ given by (6), with τ_Q being the time for cell division, and γ_Q the apoptotic rate during mitosis. See Bernard et al. (2003) for a detailed derivation. Here, we remove the dependence of γ_Q upon G-CSF as the HSC population is relatively stable and infrequently dividing (Riether et al. 2015, Durand and Charbord 2010) and, to our knowledge, no direct evidence of G-CSF's action upon HSC apoptosis currently exists. Craig et al. (2015) uses

$$A_Q(t) = 2\exp\left[-\int_{t-\tau_Q}^{t}\gamma_Q(s)\mathrm{d}s\right], \tag{18}$$

and in the absence of chemotherapy we take the apoptotic rate γ_Q to be constant so this becomes (7).

3.2 A Physiologically Constructed Pharmacokinetic G-CSF Model

A new pharmacokinetic model of G-CSF already stated in (4), (5) is used to model the concentrations of both unbound and bound G-CSF. We do not distinguish between endogenous and exogenous G-CSF in the model, which constrains us to only consider biosimilar forms of exogenous G-CSF. Accordingly, we focus on filgrastim, the most widely available form of exogenous G-CSF. However, other less common forms of biosimilar exogenous G-CSF are available and include lenograstim and Nartograstim® (Molineux et al. 2012). The pegylated form of rhG-CSF has greatly reduced renal clearance relative to endogenous G-CSF, which would require a different model, so we will not consider it in this work.

In Eqs. (4), (5) G_1 is the concentration of freely circulating G-CSF and G_2 is the concentration of G-CSF which is bound to receptors on the neutrophils. Since the bone marrow is well perfused G-CSF can bind to mature neutrophils in the marrow reservoir as well as neutrophils in circulation. In the model k_{ren} denotes the nonsaturable removal rate of circulating G-CSF (mainly renal). k_{int} denotes the removal rate of bound G-CSF, which we refer to as the effective internalization rate. This term models the removal of bound G-CSF both by internalization after binding and through the removal of the neutrophil itself from circulation (along with its bound G-CSF molecules). k_{12} is the rate of binding of free G-CSF to the neutrophils, and Pow is the effective binding coefficient. The G-CSF receptor has a 2:2 stoichiometry in in vitro studies (Layton and Hall 2006), so a simple chemical reaction model would suggest Pow = 2. However,

the number of ligands binding to a receptor only provides an upper bound on the corresponding Hill coefficient (Santillán 2008) and so we use an effective binding coefficient Pow $\in [1, 2]$.

In our model the bound G-CSF concentration, G_2, is saturable, with the capacity of this compartment being $V[N_R(t) + N(t)]$. Only if every receptor on every neutrophil in the reservoir and circulation was bound to two G-CSF molecules would G_2 equal $V[N_R(t) + N(t)]$. Thus, the removal rate of neutrophils by internalization is saturable. G-CSF also binds to immature neutrophils and precursors, which will be important for the pharmacodynamics, but since these cells are fewer in number and/or have fewer receptors than the mature neutrophils we neglect this effect on the pharmacokinetics. Finally, k_{21} is the rate of unbinding (transformation from bound G-CSF to circulating G-CSF), and $I_G(t)$ denotes exogenous administration of G-CSF, discussed in Sect. 3.5.

If we were to assume that there is no net transfer between the bound and circulating G-CSF then letting $\tilde{N}(t) = [N_R(t) + N(t)]$, Eqs. (4), (5) imply

$$k_{12}(V\tilde{N}(t) - G_2)G_1^{\text{Pow}} - k_{21}G_2 \approx 0. \tag{19}$$

Rearranging (19) we obtain

$$G_2(t) \approx \frac{[G_1(t)]^{\text{Pow}}}{[G_1(t)]^{\text{Pow}} + k_{21}/k_{12}} V\tilde{N}(t).$$

Now, adding (4) and (5)

$$\frac{\mathrm{d}}{\mathrm{d}t}(G_1 + G_2) \approx I_G(t) + G_{\text{prod}} - k_{\text{ren}}G_1 - k_{\text{int}}G_2,$$

and assuming that $G_1 \gg G_2$ and that $\frac{\mathrm{d}}{\mathrm{d}t}(G_1 + G_2) \approx \frac{\mathrm{d}}{\mathrm{d}t}G_1$, and finally replacing the $\approx$ by an equality we obtain

$$\frac{\mathrm{d}}{\mathrm{d}t}G_1 = I_G(t) + G_{\text{prod}} - k_{\text{ren}}G_1 - k_{\text{int}}V\tilde{N}(t)\frac{[G_1(t)]^{\text{Pow}}}{[G_1(t)]^{\text{Pow}} + k_{21}/k_{12}}. \tag{20}$$

Equations similar to (20) have been used to model G-CSF pharmacokinetics in many papers including Craig et al. (2015), Brooks et al. (2012), Foley and Mackey (2009b), Krzyzanski et al. (2010), Krinner et al. (2013), and Wang et al. (2001), but usually with $\tilde{N}(t) = N(t)$ the concentration of circulating neutrophils, as opposed to $\tilde{N}(t) = [N_R(t) + N(t)]$ as (4), (5) suggest.

The usual derivation of (20) is from the law of mass action, but this is equivalent to the assumption (19) that the bound and circulating G-CSF are in quasi-equilibrium. However, the equilibrium hypothesis (19) cannot hold at homeostasis, since if (19) holds and $k_{\text{int}} > 0$ then $\frac{\mathrm{d}}{\mathrm{d}t}G_2 < 0$ which is contradictory. Clinical evidence (Sarkar et al. 2003; Terashi et al. 1999) suggests that at homeostasis, binding and internalization is the dominant removal mechanism for G-CSF, so not only does (19) not hold but the net transfer from unbound to bound G-CSF should be more than $0.5 \times G_{\text{prod}}$. Another important situation where (19) will fail is during exogenous administration of G-CSF,

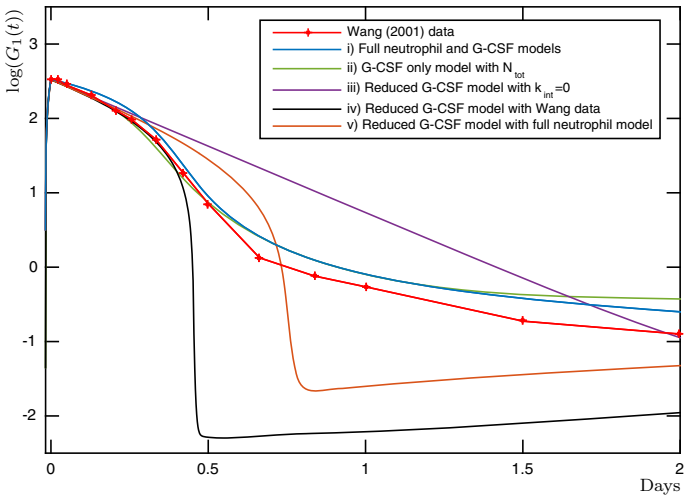

Fig. 2 Data from Wang et al. (2001) for G-CSF concentrations after a 750-μg 25-min IV infusion and five different simulations: (*i*) the full neutrophil and G-CSF model (1)–(5) (*ii*) the G-CSF only model (68), (69), (*iii*) the reduced G-CSF model (20) with $k_{\text{int}} = 0$, (*iv*) the reduced G-CSF model (20) with $k_{\text{int}} = 30$ and $\tilde{N}(t) = N(t)$ and neutrophil concentrations taken from the Wang et al. (2001) and (*v*) the full neutrophil model (1)–(3) and the reduced G-CSF model (20) with $k_{\text{int}} = 25$ and $\tilde{N}(t) = [N_R(t) + N(t)]$. In (*ii*) $N_{\text{tot}} = 4.1457$ and G_2^* and G_{prod} are determined by Eqs. (74) and (76), respectively. In (*ii*), (*iv*), and (*v*) $k_{\text{ren}} = 4.12$ and G_{prod} is determined by (20). All other parameters take values specified in the third columns of Tables 1 and 2

which will initially increase the concentration of unbound G-CSF (often by orders of magnitude).

Figure 2 illustrates some of the issues involved in modelling the kinetics of G-CSF. This figure shows data from a 750-μg intravenous (IV) infusion digitized from Fig. 6 of Wang et al. (2001), along with a number of simulations of the protocol using different G-CSF kinetic models. The data in Fig. 2 seem to have at least two different slopes, suggesting that the G-CSF time course could be approximated by the sum of two exponentials. This naturally leads to two compartment pharmacokinetic models (DiPiro et al. 2010). Such a two-compartment G-CSF model was previously considered by Kuwabara et al. (1994) for Nartograstim®. Consistent with general two-compartment models in pharmacology, the two compartments corresponded to the blood and the tissues, and generic saturable and nonsaturable removal of the G-CSF both occurred from the blood compartment. This differs from our model where elimination occurs from the two compartments (which instead represent unbound and bound G-CSF concentrations), both of which are subject to linear elimination. By contrast, in our model one compartment is saturable with nonsaturable elimination (the bound G-CSF), which corresponds to known G-CSF removal mechanisms. The assignment of elimination to the first or second compartments also has significant effects on the estimation of corresponding pharmacokinetic parameters so the mis-characterization of these elimination dynamics could have significant effects on the model's predictions and behaviors [73].

The circulating G-CSF concentration time course for a simulation of our full model (1)–(5) tracks the measured G-CSF data very closely in Fig. 2—curve i. It slightly overestimates the G-CSF, but it is important to note that the data points are average values from a number of subjects and we will see in Sect. 4.2 that the G-CSF concentrations predicted by our model fall well within recorded ranges for a variety of administration protocols.

Also shown in Fig. 2 is a simulation of a simplified version of the G-CSF Eqs. (4), (5) where the time-dependent neutrophil term $[N_R(t)+N(t)]$ is replaced by a constant N_{tot}, so the G-CSF kinetic equations become independent of the neutrophil dynamics (Fig. 2—curve ii). The resulting equations are stated as (68), (69) in Sect. 4.2 where they are used to determine the pharmacokinetic parameters that appear in (4), (5). The constant N_{tot} can be thought of as a time average of the term $[N_R(t) + N(t)]$. As shown in Fig. 2, this stand-alone simplified G-CSF model gives G-CSF concentrations very close to those of the full model, which justifies using it to determine the kinetic parameters.

Three different simulations of the single G-CSF Eq. (20) are also shown in Fig. 2 to illustrate the difficulties in dealing with reduced models. One simulation has $k_{\text{int}} = 0$ (Fig. 2—curve iii) so that the elimination of G-CSF is purely renal, and it is clear that the nuances of the G-CSF kinetics are lost.

A simulation of (20) with $k_{\text{int}} > 0$ and $\tilde{N}(t) = N(t)$ (with values for $N(t)$ taken from the Wang data) gives even worse results than the purely renal elimination case (Fig. 2—curve iv). The problem with this model is that for the first few hours, while the neutrophil concentration is low, the elimination of the G-CSF is mainly renal and the solution closely tracks the results from the purely renal elimination simulation. But as soon as the circulating neutrophil concentrations get high enough the elimination of G-CSF by binding becomes dominant and quickly drives the G-CSF concentration to very low levels. Similar results are seen if our full neutrophil model (1)–(3) is coupled to (20) with $\tilde{N}(t) = [N_R(t) + N(t)]$ (Fig. 2—curve v).

The tendency of the internalization term to quickly drive the G-CSF concentrations down, along with the practice of fitting parameters in linear scales, resulted in several previous models using versions of (20) to take kinetic parameters for which the elimination of G-CSF is always renal dominated. This is seen both when the G-CSF kinetics is coupled to physiological models as in Brooks et al. (2012), Craig et al. (2015) and when using traditional empirical models as in Wang et al. (2001), Krzyzanski et al. (2010), which consequently all have elimination dynamics which are always renal dominated.

This is true in both the models of Craig et al. (2015), which used (20) with $\tilde{N}(t) = N(t)$, and Krzyzanski et al. (2010) which used an equation similar to (20) but taking account of binding to all available receptors. In both, elimination by internalization is included in the mathematical models but occurs at an insignificant rate compared to the renal elimination, contrary to the clinical understanding that elimination of G-CSF by internalization is the dominant removal mechanism at homeostasis.

From our numerical experiments it seems impossible to fit the single G-CSF Eq. (20) to data when $\tilde{N}(t)$ is taken to be $N(t)$. The mature marrow neutrophil reservoir is an order of magnitude larger than the total blood neutrophil pool, and the receptors on the

mature neutrophils need to be taken into account in the kinetics as in (4), (5) to obtain a good fit to data. But taking account of all the receptors is not sufficient to obtain a model that fits the physiology closely. This is evidenced by the very poor fit obtained in Fig. 2 when coupling our neutrophil model to the reduced G-CSF Eq. (20) with $\tilde{N}(t) = [N_R(t) + N(t)]$, and also from models such as that of Krzyzanski et al. (2010) that take account of the G-CSF receptors in marrow, but still obtain renal dominated kinetics.

The study of congenital diseases like cyclical neutropenia (CN)—an inherently oscillatory and dynamic disease—and exogenous dosing regimens (such as during chemotherapy) necessitates that the dynamics of G-CSF be well characterized. Hence, we use the more realistic model (4), (5) for G-CSF pharmacokinetics rather than the single equation reduction (20).

3.3 Modelling Granulopoiesis

The first term on the right-hand side of (2) gives the rate that mature neutrophils enter the bone marrow reservoir at time t and is obtained by modelling the differentiation of stem cells at time $t - \tau_N(t)$ through mitosis of neutrophil precursors to time $t - \tau_N(t) + \tau_{N_P} = t - \tau_{N_M}(t)$ followed by maturation of the cells until time t. The time variation of $\tau_N(t)$ and $\tau_{N_M}(t)$ is solution dependent, so this term involves state-dependent delays. Granulopoiesis models incorporating state-dependent delay have been employed before in Foley and Mackey (2009b), Foley and Mackey (2009a), and Brooks et al. (2012), but the derivation of those models was inaccurate and they missed the important $V_{N_M}(G_1(t))/V_{N_M}(G_1(t - \tau_{N_M}(t)))$ term. Here we will show in detail how the mitotic and maturation stages of the neutrophil precursors can be modelled by age-structured PDE models, whose solution by the method of characteristics leads to the state-dependent delay terms in (2).

We do not model the cell-cycle process during mitosis, nor do we differentiate between the different maturation stages of dividing cells (myeloblasts, promyelocytes, myelocytes). Rather, to simplify the modelling and the resulting differential equations we model mitosis as an exponential process from the moment the HSC commits to differentiate to the end of the mitosis. The proliferation rate η_{N_P} is assumed to be independent of which stage in mitosis the cell has reached. There is evidence that the cytokine G-CSF affects the differentiation of HSCs and the effective proliferation rate during mitosis, as explained in Endele et al. (2014), and so we allow both the differentiation rate κ and the proliferation rate η_{N_P} to vary with G_1, the circulating G-CSF, as shown in Eqs. (8), (9), and explained in Sect. 3.4.

We let $n_p(t, a)$ be the cell density as a function of time t and age a during proliferation. We assume that cells age at a constant rate, $\dot{a} = 1$, from age 0 to age τ_{N_P}, so τ_{N_P} is also the time period that cells spend in proliferation, and the proliferation rate is $\tau_{N_P}(G_1(t))$. Then, differentiating,

$$\eta_{N_P}(G_1(t))n_p(t,a) = \frac{\mathrm{d}n_p}{\mathrm{d}t} = \frac{\partial n_p}{\partial t} + \frac{\mathrm{d}a}{\mathrm{d}t}\frac{\partial n_p}{\partial a} = \frac{\partial n_p}{\partial t} + \frac{\partial n_p}{\partial a}$$

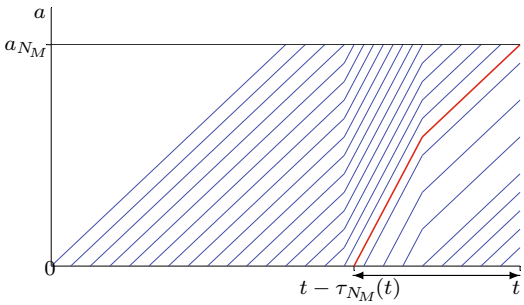

Fig. 3 During maturation the aging rate is variable with $\dot{a}(t) = V_{N_M}(G_1(t))$, so age is not trivially related to time, and the maturation time $\tau_{N_M}(t)$ is variable

so the age-structured PDE model for proliferation is

$$\frac{\partial n_p}{\partial t} + \frac{\partial n_p}{\partial a} = \eta_{N_P}(G_1(t))n_p(t,a), \quad t \geqslant 0, \quad a \in [0, \tau_{N_P}], \tag{21}$$

which by the method of characteristics has solution

$$n_p(t,a) = n_p(t-a,0)\exp\left[\int_{t-a}^{t} \eta_{N_P}(G_1(s))ds\right], \ t \geqslant 0, \ a \in [0, \min\{t, \tau_{N_P}\}]. \tag{22}$$

If $\tau_{N_P} \geqslant a > t > 0$ the solution depends on the initial condition $n_p(0, a-t)$, but a similar expression applies. We will use homeostatic initial conditions throughout, so the solution in (22) is all that is required (Fig. 3).

We model the maturing neutrophil precursors (metamyelocytes and bands) as a single homogeneous compartment. There is evidence that G-CSF affects the time that cells spend in maturation (Spiekermann et al. 1997; Basu et al. 2002) and the speedup in maturation has been measured experimentally (Price et al. 1996). Since the exact mechanism by which G-CSF affects maturation time is unknown, we will model this process by decoupling time from age and demanding that cells age by an amount a_{N_M}, but allowing them to mature at a variable aging rate $\dot{a}(t) = V_{N_M}(G_1(t))$ where $V_{N_M}(G_1)$ is a monotonically increasing function with $V_{N_M}(0) > 0$ and $\lim_{G_1 \to \infty} V_{N_M}(G_1) = V_{\max} < \infty$.

See Sect. 3.4 for further discussion of the function $V_{N_M}(G_1)$. We assume that the rate of cell death, γ_{N_M}, during maturation is constant independent of the concentration of G-CSF.

We let $n_m(t,a)$ be the cell density as a function of time t and age a during maturation for $t \geqslant 0$ and $a \in [0, a_{N_M}]$. Then the age-structured maturation model is

$$\frac{\partial n_m}{\partial t} + V_{N_M}(G_1(t))\frac{\partial n_m}{\partial a} = \frac{\partial n_m}{\partial t} + \frac{\mathrm{d}a}{\mathrm{d}t}\frac{\partial n_m}{\partial a} = \frac{\mathrm{d}n_m}{\mathrm{d}t} = -\gamma_{N_M} n_m(t,a). \tag{23}$$

The characteristics are defined by $\dot{a} = V_{N_M}(G_1(t))$, and along characteristics for $t \geqslant \tau_{N_M}(t)$ we obtain

$$n_m(t, a_{N_M}) = n_m(t - \tau_{N_M}(t), 0)e^{-\gamma_{N_M}\tau_{N_M}(t)}. \tag{24}$$

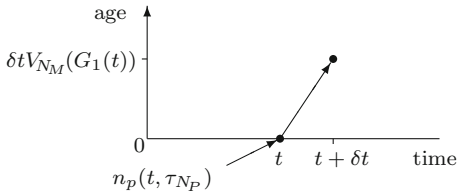

Fig. 4 Transition from proliferation to maturation

Age-structured PDE models have been used in hematopoiesis models many times previously (Lei and Mackey 2011; Foley and Mackey 2009b; Colijn and Mackey 2005b; Craig et al. 2015), but special care needs to be taken to interpret $n_m(t,a)$ when the maturation has variable velocity, or an incorrect solution will be obtained (Fig. 4).

Cells which mature at time t enter maturation at time $t-\tau_{N_M}(t)$ and so differentiated from HSCs at time $t-\tau_{N_M}(t)-\tau_{N_P}=t-\tau_N(t)$. The rate at which cells differentiate at time $t-\tau_N(t)$ is $\kappa(G_1(t-\tau_N(t)))Q(t-\tau_N(t))$, and hence,

$$n_p(t-\tau_N(t),0)=\kappa(G_1(t-\tau_N(t)))Q(t-\tau_N(t)).$$

Then by (22)

$$\begin{aligned} n_p(t-\tau_{N_M}(t),a_{N_M}) &= n_p(t-\tau_N(t),0)\exp\left[\int_{t-a_{N_M}}^{t}\eta_{N_P}(G_1(s))\mathrm{d}s\right] \\ &= \kappa(G_1(t-\tau_N(t)))Q(t-\tau_N(t))\exp\left[\int_{t-a_{N_M}}^{t}\eta_{N_P}(G_1(s))\mathrm{d}s\right]. \end{aligned} \tag{25}$$

To obtain the boundary condition for the maturation phase, note that $n_p(t,\tau_{N_P})$ is the rate at which cells leave proliferation and enter maturation. Hence, to leading order, $n_p(t,\tau_{N_P})\delta t$ cells enter maturation in the time interval $[t,t+\delta t]$. Cells that enter maturation at time t will already have age $V_{N_M}(G_1(t))\delta t$ by time $t+\delta t$. Since $n_p(t,a)$ and $n_m(t,a)$ describe the density of cells in the proliferation and maturation phases, to avoid the spontaneous creation or destruction of cells at the transition between proliferation and maturation we require

$$\int_0^{V_{N_M}(G_1(t))\delta t} n_m(t+\delta t,a)\mathrm{d}a-\int_t^{t+\delta t} n_p(t,\tau_{N_P})\mathrm{d}t=\mathcal{O}(\delta t^2).$$

Then

$$\begin{aligned} V_{N_M}(G_1(t))n_m(t,0) &= \lim_{\delta t\to 0}\frac{1}{\delta t}\int_0^{V_{N_M}(G_1(t))\delta t} n_m(t+\delta t,a)\mathrm{d}a \\ &= \lim_{\delta t\to 0}\frac{1}{\delta t}\int_t^{t+\delta t} n_p(t,\tau_{N_P})\mathrm{d}t = n_p(t,\tau_{N_P}), \end{aligned} \tag{26}$$

and hence, the boundary condition for the maturation compartment is

$$n_m(t-\tau_{N_M}(t),0) = n_p(t-\tau_{N_M}(t),\tau_{N_P})/V_{N_M}(G_1(t-\tau_{N_M}(t))). \tag{27}$$

Combining (24), (25), (27), and (14) we obtain

$$\begin{aligned} n_m(t,a_{N_M}) &= \frac{n_p(t-\tau_{N_M}(t),\tau_{N_P})}{V_{N_M}(G_1(t-\tau_{N_M}(t)))} e^{-\gamma_{N_M}\tau_{N_M}(t)} \\ &= \frac{\kappa(G_1(t-\tau_N(t))Q(t-\tau_N(t))}{V_{N_M}(G_1(t-\tau_{N_M}(t)))} \exp\left[\int_{t-\tau_N(t)}^{t-\tau_{N_M}(t)} \eta_{N_P}(G_1(s))\mathrm{d}s - \gamma_{N_M}\tau_{N_M}(t)\right] \\ &= \frac{\kappa(G_1(t-\tau_N(t)))Q(t-\tau_N(t))}{V_{N_M}(G_1(t-\tau_{N_M}(t)))} A_N(t). \end{aligned} \tag{28}$$

Again because of the variable aging rate there is a correction factor to apply to $n_m(t,a_{N_M})$ to obtain the rate that cells leave maturation. To calculate this rate notice that cells which reach age a_{N_M} at time t have age $a_{N_M} - V_{N_M}(G_1(t))\delta t + \mathcal{O}(\delta t^2)$ at time $t-\delta t$. Thus, the number of neutrophils that mature in the time interval $[t-\delta t, t]$ is

$$\int_{a_{N_M}-V_{N_M}(G_1(t))\delta t}^{a_{N_M}} n_m(t-\delta t,a)\mathrm{d}a + \mathcal{O}(\delta t^2) = V_{N_M}(G_1(t))n_m(t,a_{N_M})\delta t + \mathcal{O}(\delta t^2).$$

Hence, the rate that cells leave maturation is $V_{N_M}(G_1(t))n_m(t,a_{N_M})$, which using (28) can be written as

$$\kappa(G_1(t-\tau_N(t)))Q(t-\tau_N(t))A_N(t)\frac{V_{N_M}(G_1(t))}{V_{N_M}(G_1(t-\tau_{N_M}(t)))}, \tag{29}$$

which is the first term on the right-hand side of (2). The correction factor $V_{N_M}(G_1(t))/V_{N_M}(G_1(t-\tau_{N_M}(t)))$ was omitted from the state-dependent DDE models in Foley and Mackey (2009b) and Brooks et al. (2012).

3.4 G-CSF Pharmacodynamics

G-CSF, in concert with many other cytokines, regulates important parts of granulopoiesis. The precise mechanisms by which it does this are not fully understood (and would probably be beyond the level of detail that we would want to model mathematically even if they were), but it is known that G-CSF acts along several signalling pathways in complex processes which activate and generate secondary signals that regulate neutrophil production (Greeenbaum and Link 2011; Semerad et al. 2002; Ward et al. 1998).

The initiation of signalling pathways and the transfer of the resulting signals responsible for the various effects of a given drug may be driven directly by receptor binding

and/or the internalization of the drug. Assuming the rate at which a drug is internalized is proportional to its bound concentration, we do not need to distinguish between the different possible pathways and will use the concentration of the bound drug to drive the pharmacodynamics and produce the effects in the body.

Many previous models applied the cytokine paradigm mentioned in the introduction to model cytokine effects directly from the circulating neutrophil concentrations. For example in Colijn and Mackey (2005a), Colijn and Mackey (2005b), Foley and Mackey (2009b), Lei and Mackey (2011), Brooks et al. (2012), and Craig et al. (2015), the differentiation function was taken to be a monotonically decreasing function of the circulating neutrophil concentration. Some authors preferred instead to introduce simplified pharmacodynamic models using direct and indirect PD effects related to the concentration of unbound G-CSF (Wang et al. 2001; Shochat et al. 2007), while other more detailed approaches have also been studied (Scholz et al. 2012; Vainstein et al. 2005; Vainas et al. 2012).

The cytokine paradigm breaks down when G-CSF is given exogenously. Immediate responses of the hematopoietic system to G-CSF administration include releasing neutrophils from the marrow reservoir into circulation, and increasing the maturation speed of neutrophils, so the circulating concentration of neutrophils and the total number of neutrophils in the reservoir and circulation both increase, which results in G-CSF and neutrophil concentrations being high concurrently. Consequently, we will use G-CSF concentrations from (4), (5) to directly model the pharmacodynamic effects of G-CSF on the differentiation rate of HSCs κ, the effective proliferation rate of neutrophil precursors in mitosis η_{N_P}, the aging rate of maturing neutrophils V_{N_M}, and the release rate of neutrophils from the bone marrow reservoir φ_{N_R}.

We use Hill and Michaelis–Menten functions to model the G-CSF dependency of these effects. There is some disagreement in the literature over exactly which cytokines are important in different parts of the process, and we may be assigning some effects to G-CSF that are actually due to GM-CSF or one of the other myriad of cytokines that regulate granulopoiesis. If these other cytokines are mostly in quasi-equilibrium with G-CSF, using G-CSF as a cipher for all the cytokines should produce very similar effects without the extraordinary complexity that would be inherent in modelling each one of the cytokines.

Mammalian studies (Hammond et al. 1991; Bugl et al. 2012; Lui et al. 2013) reveal that neutrophils are still produced even in the absence of G-CSF, presumably because other cytokines are acting. Accordingly, we will construct our effects functions to have nonzero activity even in the complete absence of G-CSF. Moreover, in Sect. 4.3 we will consider the mathematics in the case of G-CSF knockout with our model to derive a parameter constraint to reduce the number of unknown parameters.

Recall that the concentration of G-CSF bound to mature neutrophils satisfies the inequality $G_2(t) \leqslant V[N_R(t) + N(t)]$ with equality only if every G-CSF receptor were bound to two G-CSF molecules. We suppose that the rate that mature neutrophils are released from the marrow reservoir into circulation is dependent on the fraction $G_{BF}(t) = G_2(t)/(V[N_R(t) + N(t)])$ of their receptors which are bound to G-CSF. The rate is then given by the Michaelis–Menten function $\varphi_{N_R}(G_{BF})$ defined by (17).

Letting

$$\varphi_{N_R}^{\text{ratio}} = \frac{\varphi_{N_R}^{\max}}{\varphi_{N_R}^{*}} > 1, \tag{30}$$

this function is also similar to the one used by Shochat et al. (2007) that was adapted in Craig et al. (2015) except that we use the fraction of bound receptors to drive the function. At homeostasis (16) and (17) imply that

$$\varphi_{N_R}(G_{BF}^{*}) = \varphi_{N_R}\left(G_2^{*}/[V(N^{*} + N_R^{*})]\right) = \varphi_{N_R}^{*}.$$

The parameter b_G defines the half-effect concentration with

$$\varphi_{N_R}(G_{BF}^{*} + b_G) = \frac{1}{2}\left(\varphi_{N_R}^{*} + \varphi_{N_R}^{\max}\right),$$

while the condition $\varphi_{N_R}(0) > 0$ implies the constraint

$$b_G > \varphi_{N_R}^{\text{ratio}} G_{BF}^{*} = \frac{G_2^{*}\varphi_{N_R}^{\text{ratio}}}{V(N_R^{*} + N^{*})}. \tag{31}$$

To model the effects of G-CSF on the differentiation, proliferation, and maturation some care must be taken. We posit that it is cytokine signalling that drives these processes, and $G_2(t)$ denotes the concentration of bound G-CSF, which is proportional to the rate that G-CSF is internalized. So it would be tempting to use $G_2(t)$ to govern these processes, and indeed initially we tried this without success. The problem is that $G_2(t)$ models the concentration of G-CSF bound to mature neutrophils in the marrow reservoir and circulation. Through (4) and (5) this gives a very good model of the removal of G-CSF from circulation because although the neutrophil progenitor cells also have G-CSF receptors, these cells are relatively few in number and have relatively few receptors, hence they can be ignored when modelling the G-CSF kinetics. However, when modelling the pharmacodynamic effects of G-CSF it appears to be crucial to take account of the binding of G-CSF to the neutrophil precursors, and it is the freely circulating G-CSF which is available to bind to the G-CSF receptors on the immature neutrophils and precursors. Consequently, we should use $G_1(t)$ to govern the cytokine dependent differentiation, proliferation, and maturation.

Another way to see that it should be the circulating G-CSF $G_1(t)$, and not the G-CSF bound to mature neutrophils $G_2(t)$ that should govern these processes is as follows. If the concentration of mature neutrophils is decreased then the concentration of bound G-CSF will also decrease because the number of receptors available to bind to will be decreased, but the concentration of unbound G-CSF will increase because the rate the G-CSF is removed by internalization is reduced. However, with a reduced concentration of neutrophils, an elevated cytokine concentration is needed to increase differentiation, proliferation, and maturation speed.

We model the differentiation rate from HSCs to neutrophil precursors using the Hill function (8). Very little is known about how the differentiation rate changes as

a function of G-CSF, but we suppose that it will not vary by orders of magnitude, since this would lead to instability in the HSC population, while the HSC population is observed to be very stable in healthy subjects (Riether et al. 2015). It is then convenient to assume that the homeostatic rate is at the midpoint of the range of possible differentiation rates so

$$\kappa^* = \frac{1}{2}\left(\kappa^{\min} + \kappa^{\max}\right). \tag{32}$$

With this assumption (8) is a standard sigmoidal Hill function with minimum differentiation rate $\kappa(0) = \kappa^{\min}$, and with $\kappa(G_1)$ increasing monotonically with G_1 and such that at homeostasis $\kappa(G_1^*) = \kappa^*$, while for large concentrations $\lim_{G_1\to\infty}\kappa(G_1) = \kappa^* + (\kappa^* - \kappa^{\min}) = \kappa^{\max}$. To ensure that neutrophils are still produced in the complete absence of G-CSF we will require that $\kappa^{\min} > 0$.

G-CSF is believed to increase the effective rate of mitosis during proliferation by reducing apoptosis. Thus, we use a monotonically increasing Michaelis–Menten function $\eta_{N_P}(G_1(t))$ defined by (9) to describe the G-CSF-dependent effective proliferation rate (which measures the difference between actual proliferation and apoptosis). This function looks a little different than the other Michaelis–Menten functions we will use, but this is simply because it has been scaled to give the correct minimal and homeostasis effects with $\eta_{N_P}(0) = \eta_{N_P}^{\min} > 0$ and $\eta_{N_P}(G_1^*) = \eta_{N_P}^*$, with $\eta_{N_P}(G_1)$ a monotonically increasing function of G_1.

Letting

$$\eta_{N_P}^{\max} = \lim_{G_1\to\infty}\eta_{N_P}(G_1) = \eta_{N_P}^* + \frac{b_{N_P}}{G_1^*}\left(\eta_{N_P}^* - \eta_{N_P}^{\min}\right),$$

we see that

$$\frac{b_{N_P}}{G_1^*} = \frac{\eta_{N_P}^{\max} - \eta_{N_P}^*}{\eta_{N_P}^* - \eta_{N_P}^{\min}},$$

so the parameter $b_{N_P} > 0$ determines the relative position of $\eta_{N_P}^* \in [\eta_{N_P}^{\min}, \eta_{N_P}^{\max}]$ with $\eta_{N_P}^* > (\eta_{N_P}^{\min} + \eta_{N_P}^{\max})/2$ when $b_{N_P} \in (0, G_1^*)$ and $\eta_{N_P}^* < (\eta_{N_P}^{\min} + \eta_{N_P}^{\max})/2$ when $b_{N_P} > G_1^*$.

G-CSF is known to affect the time that neutrophils spend in maturation (Spiekermann et al. 1997; Basu et al. 2002), an acceleration in maturation that Price et al. (1996) measured experimentally, but the mechanism by which G-CSF speeds up maturation is not well understood. We choose to model this process by decoupling time from age and demanding that cells age by an amount a_{N_M}, but allowing them to mature at a variable aging rate $\dot{a}(t) = V_{N_M}(G_1(t))$ where $V_{N_M}(G_1)$ is a monotonically increasing Michaelis–Menten function given in (10). This is similar to the form used in Craig et al. (2015) which was adopted from Foley and Mackey (2009b) and is also functionally equivalent to (17).

The aging velocity function $V_{N_M}(G_1)$ satisfies the homeostasis condition $V_{N_M}(G_1^*) = 1$, so the aging rate at homeostasis is 1. The aging rate saturates with $\lim_{G_1\to\infty} V_{N_M}(G_1) = V_{\max} \in (1, \infty)$, where b_V is the half-effect parameter with

$V_{N_M}(G_1^* + b_V) = (1 + V_{\max})/2$. We will require that $V_{N_M}(0) > 0$, which from (10) is equivalent to the constraint

$$b_V > G_1^* V_{\max}. \tag{33}$$

This ensures that the aging velocity $V_{N_M}(G_1)$ is strictly positive for all $G_1 \geqslant 0$.

Notice that, using (13)

$$\frac{\mathrm{d}}{\mathrm{d}t}(t - \tau_{N_M}(t)) = 1 - \frac{\mathrm{d}}{\mathrm{d}t}\tau_{N_M}(t) = \frac{V_{N_M}(G_1(t))}{V_{N_M}(G_1(t - \tau_{N_M}(t)))}, \tag{34}$$

and positivity of $V_{N_M}(G_1)$ assures that $t - \tau_{N_M}(t)$, and similarly $t - \tau_N(t)$, are monotonically increasing functions of t. This is important in state-dependent DDE theory for existence and uniqueness of solutions. Physiologically, it assures that cells which have exited maturation never reenters that phase.

One can conceive of other biological systems where nonmonotonic deviating arguments $t - \tau_M(t)$ would be natural. For example, aging velocity could be negative if insufficient nutrients were available to maintain the mass of an organism in a model where maturation was governed by juvenile size. In such a model there would be no output from maturation at time t if $t - \tau_M(t) < \sup_{s \leqslant t} s - \tau_M(s)$, units that would have exited maturation at time t having already done so at some previous time. However, given the lack of evidence for such mechanisms in hematopoiesis, we will always impose (33) to ensure that the aging velocity is positive.

The responses of our new model and the model of Craig et al. (2015) to exogenous administration of G-CSF are very different. With our new model both differentiation and proliferation are increased with increased G-CSF so that after some time delay the marrow reservoir gets replenished. In the previous model, the G-CSF triggered an immediate release of neutrophils from the marrow reservoir into circulation and the resulting high circulating neutrophil count would cause differentiation and proliferation to be decreased. This meant the the marrow reservoir would suffer a double depletion with increased release into circulation combined with reduced production of new mature neutrophils, which could lead to instabilities in the model that ought not to be occurring in the granulopoiesis of healthy subjects.

Since the four functions (8), (9), (10), and (17) describe the effects of G-CSF on granulopoiesis, rather than modelling the processes that lead to the effects, the parameters in these functions do not correspond to physiological quantities that can be measured directly. Nevertheless, these parameters can be determined by fitting the response of the system to experimental data as described in Sect. 4.4.

3.5 Modelling Exogenous Drug Administration

As noted following (4), $I_G(t)$ denotes the input of exogenous G-CSF. The administration of rhG-CSF (in our case filgrastim) typically takes two forms: IV infusion (where the drug is given intravenously over a period of time) or subcutaneously (injection under the skin). In the former case, the drug passes directly into the bloodstream meaning the bioavailable fraction (the percentage of the administered dose that enters the blood) is 100 %. In this case, we express the single exogenous administration as

$$I_G(t) = \begin{cases} \frac{\mathrm{Do}}{t_{\mathrm{inf}} V_d}, & t_0 \leqslant t \leqslant t_{\mathrm{inf}} \\ 0 & \text{otherwise,} \end{cases} \tag{35}$$

where Do is the administered dose, t_0 is the start of the infusion, t_{inf} is the time of infusion, and V_d is the volume of distribution. The volume of distribution is a pharmacokinetic parameter which relates the hypothetical volume a drug would occupy to the concentration observed in the plasma. It is typically calculated for a drug by dividing the administered dose by the concentration in the blood immediately following an administration for the simplest case of IV bolus administration (instantaneous administration into the blood). Drugs given subcutaneously do not immediately reach the bloodstream. Instead, a certain proportion of the medication remains in the subcutaneous tissue pool before diffusing into the plasma. Some previous studies, notably (Foley and Mackey 2009b; Brooks et al. 2012) used an extra transition compartment to model the administered G-CSF concentration in the tissues before reaching the blood and allowed for the free exchange between this central (blood) compartment and the tissue compartment. Owing to the specifics of the pharmacokinetics of filgrastim, we will instead use the following direct input functions obtained by solving the differential equation for the dose deposit compartment as in Krzyzanski et al. (2010) and Craig et al. (2015) to model subcutaneous administration as

$$I_G(t) = \begin{cases} \frac{k_a \mathrm{Do} F}{V_d} e^{-k_a(t-t_0)}, & t \geqslant t_0 \\ 0 & t < t_0, \end{cases} \tag{36}$$

where k_a is the constant of absorption, and F is the bioavailable fraction (the fraction of nonmetabolized dose which enters the system). This direct form is preferred over the two compartment method previously employed in Foley and Mackey (2009b), Brooks et al. (2012) because of the relatively small volume of distribution exhibited by filgrastim (the biosimilar exogenous form of G-CSF), which is to say that V_d is less than the standard 70 L measure of highly distributed drugs (Craig et al. 2015) and that the drug does not have a strong tendency to redistribute into the tissues.

The pharmacokinetic model of the chemotherapeutic drug (Zalypsis®) used in this paper is the same as in Craig et al. (2015). Briefly, the concentration of chemotherapeutic drug in the system is modelled using a set of four ordinary differential equations which was determined to be suitable through population pharmacokinetic analysis (Pérez-Ruixo et al. 2012). The PK model of Zalypsis® is given by

$$\begin{aligned} \frac{\mathrm{d}}{\mathrm{d}t} C_p(t) &= I_C(t) + k_{fp} C_f(t) + k_{sl_1 p} C_{sl_1}(t) - (k_{pf} + k_{psl_1} + k_{el_C}) C_p(t) \\ \frac{\mathrm{d}}{\mathrm{d}t} C_f(t) &= k_{pf} C_p(t) + k_{sl_2 f} C_{sl_2}(t) - (k_{fp} + k_{fsl_2}) C_f(t) \\ \frac{\mathrm{d}}{\mathrm{d}t} C_{sl_1}(t) &= k_{psl_1} C_p(t) - k_{sl_1 p} C_{sl_1}(t), \\ \frac{\mathrm{d}}{\mathrm{d}t} C_{sl_2}(t) &= k_{fsl_2} C_f(t) - k_{sl_2 f} C_{sl_2}(t), \end{aligned} \tag{37}$$

where C_p is the concentration in the central (blood) compartment, C_f is the concentration in the fast-exchange tissues, and C_{sl_1} and C_{sl_2} are the concentrations in

the slow-exchange tissues, k_{ij} are traditional rate constants between the ith and jth compartments ($i, j = p, f, sl_1, sl_2$), and k_{el_C} is the rate of elimination from the central compartment. We consider the chemotherapeutic drug to be administered by IV infusion. Accordingly, we set $I_C(t) = \text{Dose}_{\text{Zal}}/\Delta_t$, where Dose_{Zal} is the administered dose and Δ_t is the time of infusion, when an infusion is administered and $I_C(t) = 0$ when no infusion is given.

In contrast to the pharmacodynamic effects of G-CSF, chemotherapy has negative effects on the neutrophil (and other blood) lineages. Chemotherapy (and radiotherapy) works by disrupting the cell cycle of tumors (Maholtra and Perry 2003), but this interference also affects all cells which are dividing, including the neutrophil progenitors. The cytotoxic side effects chemotherapeutic treatment has on the neutrophils are called myelosuppression, and it is a leading cause of treatment adaptation and/or cessation for patients undergoing chemotherapy (Craig et al. 2015). Since chemotherapy's myelosuppressive action only affects cells capable of division, we model the pharmacodynamic effects of chemotherapy on the HSCs, which rarely divide, and the neutrophil progenitors in the proliferative phase, which divide regularly until they exit the mitotic phase.

Since the effects of chemotherapy on the HSCs are not clear, we model the antiproliferative effect as a simple linear increase of the rate of apoptosis experienced by these cells by replacing γ_Q in Eq. (18) by $\gamma_Q + h_Q C_p(t)$ where $C_p(t)$ is the concentration of the chemotherapeutic drug in the central blood compartment given by (37), and h_Q is a factor to be determined (as outlined in Sect. 4.5). Then (18) gives

$$A_Q(t) = 2e^{-\gamma_Q \tau_Q - h_Q \int_{t-\tau_Q}^{t} C_p(s)\mathrm{d}s}. \tag{38}$$

It is convenient to numerically implement (38) as a differential equation, and applying Leibniz's rule to (38), similar to the derivation of (15), we obtain

$$\frac{\mathrm{d}}{\mathrm{d}t} A_Q(t) = (h_Q(C_p(t-\tau_Q) - C_p(t)))A_Q(t), \tag{39}$$

and we replace (7) by (39) when chemotherapy is administered.

The second effect of chemotherapeutic drugs is to reduce the effective proliferation rate of the mitotic neutrophil progenitors. We model this by replacing η_{N_P} of (9) by

$$\eta_{N_P}^{\text{chemo}}(G_1(t), C_p(t)) = \eta_{N_P}^{\text{inf}} + \frac{\eta_{N_P}(G_1(t)) - \eta_{N_P}^{\text{inf}}}{1 + (C_p(t)/EC_{50})^{s_c}}, \tag{40}$$

which is a modification of the model used in Craig et al. (2015). Here $\eta_{N_P}^{\text{inf}}$ corresponds to the effective proliferation rate in the presence of an infinite dose of the drug. We require $\eta_{N_P}^{\text{inf}} < \eta_{N_P}^{\min}$ to ensure that effective proliferation is reduced, so $\eta_{N_P}^{\text{chemo}}(G_1(t), C_p(t)) < \eta_{N_P}^{\text{chemo}}(G_1(t))$ whenever $C_p(t) > 0$. We will allow the possibility of $\eta_{N_P}^{\text{inf}} < 0$, which would correspond to negative effective proliferation (more death than division in the mitotic phase) in the presence of very large concentrations of the chemotherapeutic drug, though we note that because the drug is cleared from circulation relatively quickly we will have $\eta_{N_P}^{\text{chemo}}(G_1(t), C_p(t)) > 0$ most of the time even

if $\eta_{N_P}^{\inf} < 0$. If $\eta_{N_P}^{\inf} \in (0, \eta_{N_P}^{\min})$ then effective cell division is reduced but never completely halted however large the concentration of the chemotherapeutic drug. EC_{50} is the concentration of chemotherapeutic drug which gives the half-maximal effect, and s_c is a Hill coefficient. The parameters h_Q, $\eta_{N_P}^{\inf}$, EC_{50}, and s_c will all be estimated using fitting techniques described in Sect. 4.5.

4 Parameter Estimation and Equation Constraints

In this section we show how our mathematical model imposes constraints on its own parameters to be self-consistent, and how experimental data can be used to determine model parameters. We begin in Sect. 4.1 by studying the model at homeostasis and deriving inequalities that the parameters must satisfy, as well as showing how experimentally measured quantities can be used to directly determine some parameters. In Sect. 4.2 we show how the G-CSF pharmacokinetic parameters can be determined using a combination of model equation constraints and parameter fitting to experimental data from single administrations of G-CSF. In Sect. 4.3, G-CSF knockout is used to derive further parameter constraints and relationships. Finally in Sect. 4.4 we show how the pharmacodynamic parameters in the neutrophil equations can be determined by fitting the model to experimental data for the circulating neutrophil concentrations after a single IV or subcutaneous administration of G-CSF.

4.1 Neutrophil Steady-State Parameter Determination and Constraints

At homeostasis let Q^* be the stem cell concentration and denote the sizes of the four neutrophil compartments at homeostasis by N_P^* (proliferation), N_M^* (maturation), N_R^* (marrow reservoir), N^* (total blood neutrophil pool), and the average time that a cell spends in one of these stages at homeostasis by τ_{N_P}, a_{N_M}, $\tau_{N_R}^*$, and $\tau_{N_C}^*$, respectively. With the exception of τ_{N_P}, all of these quantities have been determined experimentally, but unfortunately only τ_{N_P} and a_{N_M} actually appear in our model. In this section we show that our model imposes some constraints on the values of these parameters, and also how the values of κ^*, N_P^*, N_M^*, N_R^*, N^*, a_{N_M}, $\tau_{N_R}^*$, and $\tau_{N_C}^*$ can be used through the model to determine values for the parameters τ_{N_P}, $\eta_{N_P}^*$, γ_{N_M}, γ_{N_R}, γ_N, and $\varphi_{N_R}^*$ which do appear in the model in Sect. 2.

At homeostasis Eqs. (1)–(3) become

$$0 = -\big(\kappa^* + \kappa_\delta + \beta(Q^*)\big)Q^* + A_Q^*\beta(Q^*)Q^*, \tag{41}$$

$$\kappa^* Q^* A_N^* = (\varphi_{N_R}^* + \gamma_{N_R})N_R^*, \tag{42}$$

$$\varphi_{N_R}^* N_R^* = \gamma_N N^*. \tag{43}$$

Equation (41) has the trivial solution $Q^* = 0$ with other solutions given by

$$\kappa^* + \kappa_\delta = (A_Q^* - 1)\beta(Q^*) \tag{44}$$

To the best of our knowledge, there is no experimental data to determine the relative rates of differentiation to the three cell lines (erythrocytes, neutrophils, and thrombocytes) at homeostasis. In the absence of any evidence to the contrary, we will assume that these are all equal. Since κ^* denotes the differentiation rate to the neutrophil line and κ_δ differentiation to erythrocyte and thrombocyte precursors we obtain

$$\kappa^* = \tfrac{1}{2}\kappa_\delta = \tfrac{1}{3}(A_Q^* - 1)\beta(Q^*). \tag{45}$$

At homeostasis neutrophil precursors are assumed to enter the mitotic phase at rate $\kappa^* Q^*$. They then proliferate at a rate $\eta_{N_P}^*$ for a time τ_{N_P}. The total number of cells in the proliferative phase at homeostasis is thus

$$N_P^* = \int_0^{\tau_{N_P}} \kappa^* Q^* e^{\eta_{N_P}^* s}\,\mathrm{d}s = \kappa^* Q^* \frac{e^{\eta_{N_P}^* \tau_{N_P}} - 1}{\eta_{N_P}^*}, \tag{46}$$

and cells leave proliferation and enter maturation at a rate R_P^* given by

$$R_P^* = \kappa^* Q^* e^{\eta_{N_P}^* \tau_{N_P}}. \tag{47}$$

At homeostasis from (10) we have $V_{N_M}(G_2^*) = 1$, and thus from (11), the time spent in maturation at homeostasis is a_{N_M}. The number of cells of age s for $s \in [0, a_{N_M}]$ in the maturation phase is then $\kappa^* Q^* \exp(\eta_{N_P}^* \tau_{N_P} - \gamma_{N_M} s)$, and the total number of cells in the maturation phase is

$$N_M^* = \int_0^{a_{N_M}} \kappa^* Q^* e^{\eta_{N_P}^* \tau_{N_P} - \gamma_{N_M} s}\,\mathrm{d}s = \kappa^* Q^* e^{\eta_{N_P}^* \tau_{N_P}} \frac{1 - e^{-\gamma_{N_M} a_{N_M}}}{\gamma_{N_M}}. \tag{48}$$

Writing

$$A_N^* = \exp\bigl(\eta_{N_P}^* \tau_{N_P} - \gamma_{N_M} a_{N_M}\bigr), \tag{49}$$

which corresponds to (14) at homeostasis, we can rewrite (48) as

$$N_M^* = \kappa^* Q^* A_N^* \frac{e^{\gamma_{N_M} a_{N_M}} - 1}{\gamma_{N_M}}. \tag{50}$$

Now the rate at which cells leave the maturation phase is

$$\kappa^* Q^* e^{\eta_{N_P}^* \tau_{N_P} - \gamma_{N_M} a_{N_M}} = \kappa^* Q^* A_N^*.$$

The average time, $\tau_{N_C}^*$, that neutrophils spend in circulation in the blood (in the total blood neutrophil pool) has been measured a number of times. However, what

is actually measured is the half-removal time, $\tau_{1/2}$, which gives γ_N, the removal rate from circulation by

$$\gamma_N = \frac{1}{\tau^*_{N_C}} = \frac{\ln 2}{\tau_{1/2}}. \tag{51}$$

Equation (43) ensures that at homeostasis the rate neutrophils leave the reservoir and enter circulation equals the rate at which they are removed from circulation. From this we obtain

$$\varphi^*_{N_R} = \frac{\gamma_N N^*}{N^*_R}. \tag{52}$$

The rate at which neutrophils exit the mature marrow reservoir is given by $(\varphi^*_{N_R} + \gamma_{N_R})N^*_R$ where $\varphi^*_{N_R}$ is the transition rate constant for cells entering circulation and γ_{N_R} is the random death rate. Thus, the average time that cells spend in the reservoir at homeostasis is

$$\tau^*_{N_R} = \frac{1}{\varphi^*_{N_R} + \gamma_{N_R}}. \tag{53}$$

Hence, the random death rate in the reservoir, $\gamma_{N_R} \geqslant 0$, is given by

$$\gamma_{N_R} = \frac{1}{\tau^*_{N_R}} - \varphi^*_{N_R}, \tag{54}$$

and we require that

$$\tau^*_{N_R}\varphi^*_{N_R} \leqslant 1 \tag{55}$$

to ensure that $\gamma_{N_R} \geqslant 0$. That said, using (51) and (52), we can rewrite (55) as

$$\frac{\tau^*_{N_R}}{\tau^*_{N_C}} \leqslant \frac{N^*_R}{N^*}. \tag{56}$$

The apoptosis rate during the maturation phase, $\gamma_{N_M} \geqslant 0$, is calculated by eliminating $\kappa^* Q^* A^*_N$ from (42) and (50). Also making use of (54), we obtain

$$F_M(\gamma_{N_M}) := N^*_R(e^{\gamma_{N_M} a_{N_M}} - 1) - \gamma_{N_M}\tau^*_{N_R}N^*_M = 0. \tag{57}$$

It is easy to see that $F_M(0) = 0$ and hence $\gamma_{N_M} = 0$ is one solution of (57). Since $F''_M(\gamma) > 0$ for all $\gamma \geqslant 0$, if $F'_M(0) < 0$ there is a unique $\gamma_{N_M} > 0$ such that $F_M(\gamma_{N_M}) = 0$, and no positive value of γ such that $F_M(\gamma) = 0$ if $F'_M(0) \geqslant 0$. Since cell death is known to occur in the maturation compartment (see Mackey et al.

2003), we should choose our parameters so that (57) admits a solution $\gamma_{N_M} > 0$. The condition $F'_M(0) > 0$ is equivalent to

$$\frac{N_R^*}{N_M^*} < \frac{\tau_{N_R}^*}{a_{N_M}}, \tag{58}$$

and to include apoptosis in the maturation compartment our parameters must be chosen to satisfy (58).

Equation (56) can be interpreted as a lower bound on $\tau_{N_R}^*$, and (58) as an upper bound. Eliminating $\tau_{N_R}^*$ from these two bounds we find that the parameters must satisfy

$$\frac{a_{N_M}}{\tau_{N_C}^*} < \frac{N_M^*}{N^*} \tag{59}$$

for the constraints (56) and (58) to be consistent. Then $\tau_{N_R}^*$ must satisfy

$$\tau_{N_R}^* \in \left(a_{N_M} \frac{N_R^*}{N_M^*}, \tau_{N_C}^* \frac{N_R^*}{N^*} \right) \tag{60}$$

for both (56) and (58) to be satisfied as strict inequalities. All the quantities in (60) have been estimated experimentally. To be consistent with our model the values must satisfy both (59) and (60). In Sect. 5 we state parameters that satisfy these constraints. With those parameters we take $\gamma_{N_M} > 0$ to be the unique strictly positive solution to (57).

Equation (42) ensures that the rates cells enter and leave the reservoir are equal at homeostasis. Rearranging and using (52) we obtain

$$A_N^* = \frac{N_R^*}{\kappa^* Q^* \tau_{N_R}^*}, \tag{61}$$

which determines A_N^*. Now from (49) we have

$$e^{\eta_{N_P}^* \tau_{N_P}} = A_N^* e^{\gamma_{N_M} a_{N_M}}. \tag{62}$$

Then (46) implies that

$$\eta_{N_P}^* = \kappa^* Q^* \frac{e^{\eta_{N_P}^* \tau_{N_P}} - 1}{N_P^*} = \kappa^* Q^* \frac{A_N^* e^{\gamma_{N_M} a_{N_M}} - 1}{N_P^*} \tag{63}$$

and then from (62) we have

$$\tau_{N_P} = \frac{1}{\eta_{N_P}^*} \ln\left(A_N^* e^{\gamma_{N_M} a_{N_M}}\right). \tag{64}$$

In Sect. 5 we use the equations of this section to determine parameter values for our model.

4.2 Estimation of G-CSF Pharmacokinetic Parameters

Following Watari et al. (1989), Kawakami et al. (1990), Barreda et al. (2004), and Krzyzanski et al. (2010) we take the homeostasis concentration of the free circulating G-CSF to be $G_1^* = 0.025$ ng/mL. The parameter V in (5) is the same parameter V as appears in (20). But V is difficult to interpret directly from (20), and although published values are available, they vary widely between sources. For the pharmacokinetic G-CSF model (4), (5) the meaning of V is clear; it is simply the conversion factor that converts a neutrophil concentration N in units of 10^9 cells/kg of body mass, into the corresponding G-CSF concentration VN in units of nanograms per milliliter when every receptor on the neutrophils is bound.

To compute V, we first note that the molecular mass of G-CSF is 18.8 kDa = 18,800 g/mol (Krzyzanski et al. 2010) or dividing by Avogadro's constant, the equivalent weight of G-CSF is $G_{mw} = 3.12\times10^{-11}$ ng/molecule. We take the number of receptors per neutrophil to be $R = 600$, which is in the middle of the range that Barreda et al. (2004) cites, though we note that both smaller and larger numbers can be found in the literature. Then given N, the number of receptors per milliliter is

$$R \times \frac{70}{5000} \times 10^9 \times N,$$

where we assume body mass of 70 kg and 5000 mL of blood. Since two molecules bind to each receptor the maximum concentration of bound G-CSF is

$$VN = 2 \times G_{mw} \times R \times \frac{70}{5000} \times 10^9 \times N = 0.525\,\mathrm{N}\ \text{ng/mL}$$

and hence

$$V = 0.525\ (\text{ng/mL})/(10^9\ \text{cells/kg}). \tag{65}$$

Values have been published for several of the other parameters in the G-CSF Eqs. (4), (5), but these have been largely based on in vitro experiments and/or simpler G-CSF models using mixed-effects estimation techniques, and so are not directly applicable to our model (Krzyzanski et al. 2010; Wang et al. 2001; Scholz et al. 2012; Sarkar et al. 2003).

At homeostasis, Eqs. (4), (5) give

$$G_2^* = \frac{(G_1^*)^{\mathrm{Pow}}}{(G_1^*)^{\mathrm{Pow}} + (k_{\mathrm{int}} + k_{21})/k_{12}} V[N_R^* + N^*], \tag{66}$$

and

$$G_{\text{prod}} = k_{\text{ren}} G_1^* + k_{\text{int}} G_2^* = k_{\text{ren}} G_1^* + k_{\text{int}} V [N_R^* + N^*] \frac{(G_1^*)^{\text{Pow}}}{(G_1^*)^{\text{Pow}} + (k_{\text{int}} + k_{21})/k_{12}}. \quad (67)$$

Once values of k_{int}, k_{12}, k_{21}, k_{ren}, and Pow are determined as we describe below, (66) and (67) determine values for G_2^* and G_{prod}. The remaining parameters might be determined by simulating the full model with exogenous G-CSF administration and fitting the response of the model to published data for such experiments. However, that would involve also fitting the as yet undetermined pharmacodynamic parameters in Eqs. (1)–(17) which would create a very large optimization problem, with the potential for interactions between the pharmacokinetic and pharmacodynamic parameters to create a complicated functional with many local minima. To avoid this, we prefer to determine the pharmacokinetic and pharmacodynamic parameters separately. Here we determine the PK parameters by decoupling the G-CSF Eqs. (4)–(5) from the neutrophil dynamics.

There have been several studies tracking the response of the hematopoietic system to a single administration of exogenous G-CSF including Wang et al. (2001) and Krzyzanski et al. (2010).

If data were available for circulating neutrophil and marrow reservoir neutrophil concentrations as functions of time it would be possible to treat Eqs. (4)–(5) separately from the rest of the model as a system of two ordinary differential equations with $[N_R(t) + N(t)]$ treated as a known nonautonomous forcing term determined by the data. But unfortunately it is not known how to directly measure time-varying human marrow neutrophil reservoirs or bound G-CSF concentrations and such values are not reported in the literature.

In the absence of marrow neutrophil data we will decouple the G-CSF kinetic Eqs. (4)–(5) from the rest of the model by replacing the time-dependent term $[N_R(t) + N(t)]$ by the constant N_{tot} to obtain

$$\frac{\mathrm{d}}{\mathrm{d}t} G_1(t) = I_G(t) + G_{\text{prod}} - k_{\text{ren}} G_1(t) - k_{12}(N_{\text{tot}} V - G_2(t)) G_1(t)^{\text{Pow}} + k_{21} G_2(t) \quad (68)$$

$$\frac{\mathrm{d}}{\mathrm{d}t} G_2(t) = -k_{\text{int}} G_2(t) + k_{12}\big(N_{\text{tot}} V - G_2(t)\big) G_1(t)^{\text{Pow}} - k_{21} G_2(t). \quad (69)$$

In (68) and (69) the constant N_{tot} represents the constant total number of neutrophils available for G-CSF binding and will be treated as an extra parameter to be determined during the fitting. It should correspond approximately to an average value of $[N_R(t) + N(t)]$ across the time course of the data.

With data for bound G-CSF unavailable we are constrained to fit (68), (69) to data for the unbound G-CSF. To do this we use digitizations of two sets of data from Wang et al. (2001) from a 750-μg intravenous (IV) administration of G-CSF and from a subcutaneous (SC) administration of the same dose. SC administrations necessarily include the absorption kinetics of a drug, as outlined in Eq. (36), whereas

IV administrations reach the blood directly and can be modelled more simply as in (35). For these reasons, both IV and SC data were used simultaneously during the fitting procedure to best characterize the parameters. Rather than fitting directly to the data from Wang et al. (2001), to obtain robust parameter fits we took the G-CSF data from the SC and IV administrations and fit a spline through each to define functions $G^{SC}_{\rm dat}(t)$ and $G^{IV}_{\rm dat}(t)$ over the time intervals $0 \leqslant t \leqslant 2$ days for which the data were taken. With postulated parameter values we then use the MATLAB (Mathworks 2015) ordinary differential equation solver *ode45* to simulate (68), (69) over the same time interval to define functions $G^{SC}_1(t)$ and $G^{IV}_1(t)$. We measure the error between the simulated solutions and the data using the L^2 function norm defined by

$$\|G\|_2^2 = \int_0^T G(t)^2 {\rm d}t. \tag{70}$$

For the IV data which varies over orders of magnitude, as shown in Fig. 2, we use a log scale, while for the SC data a linear scale is appropriate. We define a combined error function for both simulations by

$$\text{Err} = \|\log(G^{IV}_1) - \log(G^{IV}_{\rm dat})\|_2^2 + \chi^{0.95}\|G^{SC}_1 - G^{SC}_{\rm dat}\|_2^2, \tag{71}$$

where the scale factor χ defined by

$$\chi = \frac{\max_{t\in[0,T]}\log(G^{IV}_{\rm dat}(t)) - \min_{t\in[0,T]}\log(G^{IV}_{\rm dat}(t))}{\max_{t\in[0,T]}G^{SC}_{\rm dat}(t) - \min_{t\in[0,T]}G^{SC}_{\rm dat}(t)}, \tag{72}$$

effectively rescales the data so that both datasets have equal weight. [Since $\chi < 1$ the power 0.95 in (71) works to give slightly more weight to the SC data.]

Fitting was performed using the MATLAB Mathworks (2015) *lsqcurvefit* least squares solver, with the error function Err evaluated numerically by sampling the functions at a thousand equally spaced points. It is convenient to define the constant

$$N_{\rm elim} = 1 - \frac{k_{\rm ren}G^*_1}{G_{\rm prod}} \tag{73}$$

where $N_{\rm elim}$ is the fraction of G-CSF clearance performed through internalization at homeostasis [obtained in (73) as one minus the fraction of renal clearance at homeostasis]. The estimation was performed for the G-CSF parameters: k_{12}, k_{21}, Pow, $k_{\rm int}$, the neutrophil constant $N_{\rm elim}$, and the pharmacokinetic drug parameters k_a, and F. The elimination fraction $N_{\rm elim}$ was either fixed ($N_{\rm elim} = 0.6$ and 0.8 in Table 1) or fitted (the other entries in Table 1). At each step of the optimization the candidate k_{12}, k_{21}, Pow, $k_{\rm int}$ and $N_{\rm elim}$ are used to determine the dependent parameters G^*_2, $k_{\rm ren}$, and $G_{\rm prod}$, which from (68), (69), and (73) are given by

$$G^*_2 = V N_{\rm tot}\frac{(G^*_1)^{\rm Pow}}{(G^*_1)^{\rm Pow} + (k_{21}+k_{\rm int})/k_{12}} \tag{74}$$

Table 1 Pharmacokinetic parameter estimates from the simplified G-CSF model (68), (69) for different homeostasis elimination fractions of N_{elim}

Name	Value 1	Value 2	Value 3	Value 4	Value 5	Units
N_{elim}	0.097478	0.6	0.71678	0.8	0.87358	–
k_{ren}	1.3142	0.45064	0.2456	0.16139	0.094597	days^{-1}
k_{12}	2.3004	2.2519	2.1342	2.2423	2.878	days^{-1}
k_{21}	407.1641	198.2403	168.2588	184.8658	259.8087	days^{-1}
k_{int}	394.5111	459.2721	275.2744	462.4209	632.0636	days^{-1}
Pow	1.7355	1.4418	1.4631	1.4608	1.4815	–
N_{tot}	3.9496	4.1767	4.1457	4.2009	3.606	10^9cells/kg
			Do = 750 μg, V_d = 2178.0 mL			
F	0.99752	0.75	0.75	0.75	0.98271	–
k_a	3.8154	5.2142	5.0574	5.143	4.1931	days^{-1}
Err	0.16352	0.15716	0.17901	0.18543	0.21130	–
			Do = 300 μg, V_d = 4754.7 mL			
F	1	0.63361	0.62299	0.64466	0.71424	–
k_a	6.3783	8.0804	8.0628	8.0236	7.4367	days^{-1}
			Do = 375 μg, V_d = 2322.9 mL			
F	0.89831	0.4801	0.48549	0.49964	0.57618	–
k_a	4.18161	6.7326	6.6324	6.6133	6.1259	days^{-1}

Err is defined by (71) for the 750-μg dose. As described in the text, dose-dependent drug parameters were only recalculated for the lower doses

$$k_{\text{ren}} = \left(-1 + \frac{1}{N_{\text{elim}}}\right) V k_{\text{int}} (G_1^*)^{(\text{Pow}-1)} \frac{N_{\text{tot}}}{(G_1^*)^{\text{Pow}} + (k_{21} + k_{\text{int}})/k_{12}} \tag{75}$$

$$G_{\text{prod}} = k_{\text{int}} G_2^* + k_{\text{ren}} G_1^*. \tag{76}$$

The following fitting procedure was employed. First parameters were fit from IV data for a 750-μg administration (Wang et al. 2001) on the log scale to ensure that behavior at both high and low concentrations were properly characterized. Next initial SC parameters were fit from 750-μg SC data in linear scale. Using the parameters from these two fits as seed values, we next obtain final parameter values by fitting both log-concentration IV and linear SC data simultaneously using the norm defined in (71). Finally, as the pharmacokinetic parameters related to the SC administration have been shown to be dose-dependent (Scholz et al. 2012), we re-estimate F and k_a for lower doses of 300 and 375 μg (Krzyzanski et al. 2010; Wang et al. 2001). Since V_d is typically calculated by the ratio of the dose to the initial concentration in the blood for IV administrations (DiPiro et al. 2010), we have applied the same calculation here to scale the G-CSF prediction to the first measured data point. Accordingly, the volume of distribution was recalculated to fit the administered dose. The resulting parameters are reported in Table 1.

Figure 5 shows the comparison of the solutions from the fitting procedure of the simplified model (68), (69) for the parameter set with $N_{\text{elim}} = 0.80$ from Table 1

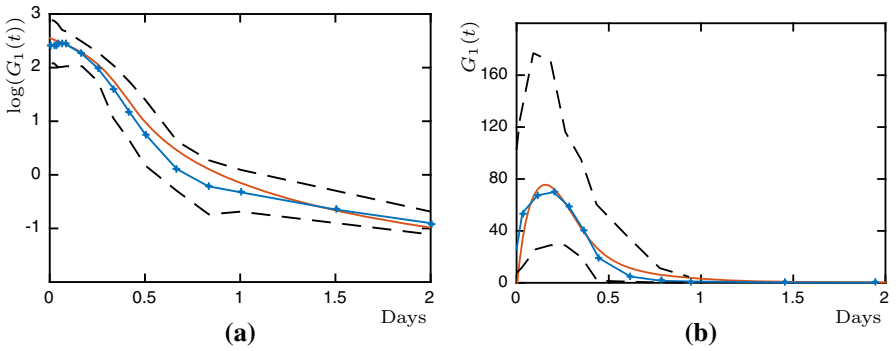

Fig. 5 G-CSF PK parameter fitting results of (68), (69) with parameter values taken from Table 1 with $N_{\text{elim}} = 0.80$. In both panels, a 750-μg dose is administered following the protocol described in Wang et al. (2001). *Blue lines with data* digitized data median values, *red solid lines* model solution with estimated parameters, *black dashed lines* maximum and minimum values of the digitized data. **a** 25-min IV infusion. **b** Subcutaneous injection (Color figure online)

to the Wang et al. (2001) data for 750-μg IV and SC doses in log and linear scales, respectively.

Figure 6a, b gives linear and log scale plots of the simulations of (68), (69) with the $N_{\text{elim}} = 0.80$ parameter set from Table 1 for an IV administration from Krzyzanski et al. (2010). In this case no fitting was performed; the Krzyzanski et al. (2010) protocol is simulated using parameters obtained from fitting to the Wang data, and a good fit to the data is still obtained. Figure 6c shows another simulation for a slightly larger SC dose, with the same G-CSF parameters (only the dose-dependent drug parameters k_a and F were fit, as already noted), and we again obtain good agreement with the data.

We characterize the parameter sets found for the simplified G-CSF model (68), (69) by the fraction N_{elim} of the G-CSF that is cleared by binding and internalization at homeostasis. For $0 \leqslant N_{\text{elim}} < 1/2$ the elimination is renal dominated at homeostasis, while for $1/2 < N_{\text{elim}} \leqslant 1$ the pharmacokinetics are internalization dominant. As already mentioned in Sect. 3.2, from a clinical standpoint, it is believed that $N_{\text{elim}} > 1/2$, while a number of previously published models including Craig et al. (2015), Krzyzanski et al. (2010), and Wang et al. (2001) have N_{elim} close to zero.

When we included N_{elim} as a parameter to be fit the results were very sensitive to the seed values used to start the optimization and had a tendency to produce parameter sets with very low or very high N_{elim} (see the $N_{\text{elim}} = 0.097$ and $N_{\text{elim}} = 0.87358$ parameter sets in Table 1), but we also found a good fit with $N_{\text{elim}} = 0.71678$ and were able to find good fits for any fixed value of N_{elim}, as shown in Fig. 5 (see Table 1 for parameter sets with $N_{\text{elim}} = 0.6$ and 0.8). Our results seem to indicate that there is at least a one parameter family of plausible parameter sets with each set characterized by the value of N_{elim}. This arises because we are fitting the simplified model (68), (69) without any data for the bound G-CSF concentrations. If the model (68), (69) were linear then parameter identifiability theory would require data from both components of the solution in order to identify unique parameters in the model. Even though (68), (69) is nonlinear, the lack of any bound G-CSF data allows us to fit the unbound G-CSF concentrations with different parameter sets, which will result

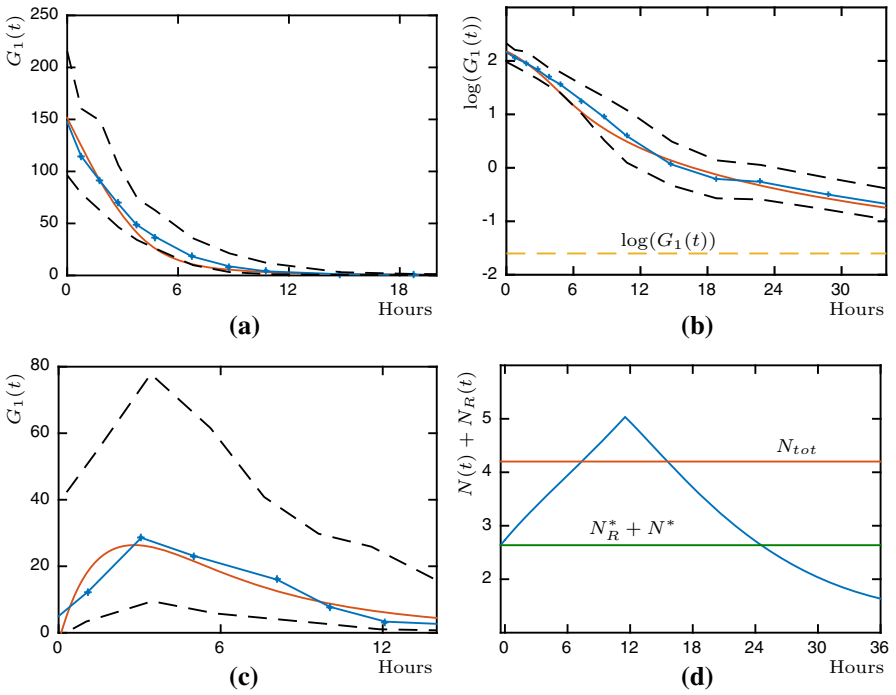

Fig. 6 G-CSF pharmacokinetic parameter fitting results of (68), (69) with parameter values taken from Table 1 with $N_{\text{elim}} = 0.80$ compared for different administration types, doses, and datasets. **a**, **b** A simulation of (68), (69) is compared to data from Krzyzanski et al. (2010) in linear and log scales. **c** A simulation compared to data from Wang et al. (2001). **d** Neutrophil concentrations (*blue line*) of the full neutrophil model (1)–(17) compared to the value of N_{tot} and $N_R^* + N^*$. **a**–**c** *Blue line with data* digitized data median values, *red solid line* model solution from estimated parameters, *black dashed lines* digitized data maximum and minimum values (Color figure online)

in different solutions for the unmeasured bound G-CSF concentrations. In Sect. 4.4 we will see that different G-CSF kinetic parameter sets will result in similar G-CSF responses, but markedly different neutrophil dynamics. The small differences in the reported errors Err in Table 1 are not sufficient alone to make a definitive judgement of which is the optimal parameter set. In the following sections we will study the response of the full system (1)–(17) not just to exogenous G-CSF but also chemotherapeutic treatment (both alone and with prophylactic exogenous G-CSF) which will lead us to conclude that the PK parameters from Table 1 with $N_{\text{elim}} = 0.80$ produce the best model responses to a variety of scenarios.

As shown in Table 1, the estimates obtained for N_{tot} are significantly larger than $[N_R^* + N^*]$. Figure 6d validates the use of the N_{tot} simplification used for (68), (69) by comparing N_{tot} to $[N_R^* + N^*]$ and to $N_R(t) + N(t)$ from the solution of the full model (1)–(17) with a 750-μg dose of G-CSF administered by a 25-min IV infusion. This demonstrates that N_{tot} is an approximate average for $[N_R(t) + N(t)]$ over most of the simulation. This, along with the similarity between the results given by (4)–(5) and the full model (as illustrated in Fig. 2) not only gives us confidence in the simplified model

(68)–(69) for estimating the G-CSF kinetic parameters, but also provides additional confirmation that the marrow reservoir neutrophils $N_R(t)$ must be included along with the total blood neutrophil pool $N(t)$ in the full kinetic G-CSF model (4)–(5) in order to reproduce the observed physiological response.

4.3 Parameter Estimates from G-CSF Knockout

Several murine studies (Bugl et al. 2012, Lui et al. 2013) have looked at the effects of G-CSF knockout by producing mice lacking G-CSF receptors and measuring the differences in circulating neutrophil counts compared to wild-type mice. The conclusion of these studies is that even in the case of complete incapacity of the neutrophils to bind with G-CSF, neutrophil counts were still between 20 and 30 % of normal levels. This is consistent with G-CSF not being the sole cytokine to regulate neutrophil production. Consequently, we will ensure that our model produces reduced but nonzero circulating neutrophil concentrations in the complete absence of G-CSF, and so in this section we consider the behavior of the equations defining neutrophil production when $G_1 \equiv G_2 \equiv 0$. In that case the four G-CSF dependent functions take values $\kappa(0) = \kappa^{\min}$, $\eta_{N_P}(0) = \eta_{N_P}^{\min}$, $V_{N_M}(0) \in (0, 1)$ [by (33)], and $\varphi_{N_R}(0) \in (0, \varphi_{N_R}^*)$ [by (31)].

We let N_{ko}^* denote the total blood neutrophil pool under G-CSF knockout and define the ratio

$$C_{ko} = N_{ko}^*/N^*. \tag{77}$$

Let $\theta = R_{\mathrm{Pko}}/R_P^*$ be the ratio of the rate of cells leaving proliferation in the absence of G-CSF to the rate of cells leaving proliferation at homeostasis. Using (47) and a similar calculation for R_{Pko} we obtain

$$\theta = \frac{R_{\mathrm{Pko}}}{R_P^*} = \frac{\kappa^{\min} Q^* e^{\tau_{N_P}\eta_{N_P}^{\min}}}{\kappa^* Q^* e^{\tau_{N_P}\eta_{N_P}^*}} = \frac{\kappa^{\min}}{\kappa^*} e^{\tau_{N_P}\eta_{N_P}^*(\mu-1)}, \tag{78}$$

where we also introduce the second auxiliary parameter

$$\mu = \eta_{N_P}^{\min}/\eta_{N_P}^* \leqslant 1, \tag{79}$$

which measures the fractional reduction in the proliferation rate at knockout. In (78) we have assumed that the number of stem cells is unchanged at knockout. Since the differentiation rate to neutrophils will be decreased from κ^* to $\kappa^{\min}$ in the absence of G-CSF, the number of stem cells will actually increase, but using (44) and (6) this increase can be calculated and is found to be less than 1 % for our model parameters.

For given values of θ, μ and $e^{\tau_{N_P}\eta_{N_P}^*}$ we will use (78) to determine the ratio $\kappa^{\min}/\kappa^*$. Since $\kappa^{\min} \leqslant \kappa^*$ [see (32)], (78) implies that $\theta \leqslant e^{\tau_{N_P}\eta_{N_P}^*(\mu-1)}$. Rearranging this gives a lower bound for μ, from which obtain the constraint

$$\mu \in \left(1 + \frac{\ln(\theta)}{\tau_{N_P} \eta^*_{N_P}}, 1\right). \tag{80}$$

Here $\mu = 1$ corresponds to a constant proliferation rate independent of G-CSF, with the reduced production of neutrophils at knockout caused by a reduction of the differentiation rate κ. If μ is equal to its lower bound then κ is constant independent of G-CSF concentration, and the reduced production of neutrophils is caused by the reduced effective proliferation rate η_{N_P}. For intermediate values of μ, both $\kappa^{\min}$ and $\eta^{\min}_{N_P}$ are reduced from their homeostasis values, and μ acts as a tuning parameter to weight the relative contribution of each mechanism with $\kappa^{\min}/\kappa^*$ a monotonically decreasing function of $\mu = \eta^{\min}_{N_P}/\eta^*_{N_P}$.

A value for θ can be computed by studying the dynamics in the absence of G-CSF after the proliferation stage. Letting N^*_{ko} and N^*_{Rko} denote the number of neutrophils at knockout in the total blood pool and in the marrow reservoir, respectively, the rate that cells enter and leave circulation should be equal implying that $\gamma_N N^*_{ko} = \varphi_{N_R}(0) N^*_{Rko}$, or

$$N^*_{Rko} = \frac{1}{\varphi_{N_R}(0)} \gamma_N N^*_{ko}. \tag{81}$$

The rate R_{Mko} that mature neutrophils are created at knockout is then equal to the rate that neutrophils enter and leave the marrow reservoir, and hence,

$$R_{Mko} = (\varphi_{N_R}(0) + \gamma_{N_R}) N^*_{Rko} = \gamma_N N^*_{ko} \left(1 + \frac{\gamma_{N_R}}{\varphi_{N_R}(0)}\right). \tag{82}$$

During G-CSF knockout, the maturation time is given by $a_{N_M}/V_{N_M}(0)$, during which cells die at a constant rate γ_{N_M} (which is not affected by G-CSF). Hence, the rate R_{Pko} that cells exit proliferation in the absence of G-CSF is related to R_{Mko} by

$$R_{\text{Pko}} e^{-\gamma_{N_M} \frac{a_{N_M}}{V_{N_M}(0)}} = R_{Mko}.$$

Thus,

$$R_{\text{Pko}} = e^{\gamma_{N_M} \frac{a_{N_M}}{V_{N_M}(0)}} R_{Mko} = \gamma_N N^*_{ko} \left(1 + \frac{\gamma_{N_R}}{\varphi_{N_R}(0)}\right) e^{\gamma_{N_M} \frac{a_{N_M}}{V_{N_M}(0)}}. \tag{83}$$

A similar calculation yields R^*_P, the rate that cells leave proliferation at homeostasis (with G-CSF), as

$$R^*_P = \gamma_N N^* \left(1 + \frac{\gamma_{N_R}}{\varphi^*_{N_R}}\right) e^{\gamma_{N_M} a_{N_M}}. \tag{84}$$

Then

$$\theta = \frac{R_{\mathrm{Pko}}}{R_P^*} = C_{ko}\frac{\varphi_{N_R}(0)+\gamma_{N_R}}{\varphi_{N_R}^*+\gamma_{N_R}}\exp\Big[a_{N_M}\gamma_{N_M}\Big(\frac{1}{V_{N_M}(0)}-1\Big)\Big], \tag{85}$$

where C_{ko} is defined by (77).

4.4 Estimating the Pharmacodynamic Parameters

We still require estimates for six parameters, μ, b_{N_P}, $V_{\max}$, b_V, b_G, and $\varphi_{N_R}^{\max}$ in the functions defining the pharmacodynamic effects of G-CSF on the neutrophil production and mobilization.

We digitized data from Wang et al. (2001) for average circulating neutrophil concentrations for 3 days following a 375- and a 750-μg 25-min IV infusion. The data also contained circulating G-CSF concentrations, but we did not use the G-CSF concentrations for fitting. As in Sect. 4.2, instead of fitting directly to the data we used it to define two continuous functions $N_{\mathrm{dat}}^{375}(t)$ and $N_{\mathrm{dat}}^{750}(t)$, one for each dose, and fit the response of the full model (1)–(17) to these functions.

The fitting is difficult because no data are available for reservoir or stem cell concentrations, and the circulating neutrophil concentrations are only measured for 3 days after the infusion. Since the proliferation time for neutrophil precursors is about a week, these data cannot be used to fit any stem cell parameters, as no cells that commit to differentiate to the neutrophil line after the infusion will reach circulation during this time (which is why we do not re-estimate any stem cell parameters in the current work). Although at homeostasis it also takes about a week for cells to traverse maturation and the marrow reservoir, these processes are greatly sped up after G-CSF administration, and cells that are in proliferation at the time of the infusion can reach circulation within a day, enabling us to estimate relevant parameters.

After 3 days the neutrophil concentrations have not returned to their homeostatic values. If parameters are fit just using this short interval of data, we found parameters which gave good fits to the circulating neutrophil concentrations over the first 3 days, but for which the neutrophil concentrations then underwent very large deviations from homeostasis values lasting months or more. There is no evidence of a single G-CSF administration destabilizing granulopoiesis (Molineux 2011). Accordingly, we will require that the fit parameters result in stable dynamics. We do this by adding artificial data points for $7 \leqslant t \leqslant 21$ days. Accordingly, we construct $N_{\mathrm{dat}}^{375}(t)$ and $N_{\mathrm{dat}}^{750}(t)$ over two disjoint time intervals as splines through the data points for $t \in [0, 3]$ and as constant functions $N_{\mathrm{dat}}^{\mathrm{dose}}(t) = N^*$ for $t \in [7, 21]$. Since we have no data for t between 3 and 7 days describing how the neutrophils return to homeostasis, we do not define values for $N_{\mathrm{dat}}^{\mathrm{dose}}(t)$ for this time interval.

For candidate parameter values, we then used MATLAB's delay differential equation solver *ddesd* (Mathworks 2015) to simulate (1)–(17) over the full 21-day time interval. This defined the functions $N^{375}(t)$ and $N^{750}(t)$, from which we were able to measure the error between the data and the simulated solutions using an L^2 function norm similar to the one defined in (70). For the disjoint time intervals, we have two

integrals to perform, and rescale them to carry equal weight and hence define

$$\|N\|_2^2 = \frac{1}{3}\int_0^3 N(t)^2 \mathrm{d}t + \frac{1}{14}\int_7^{21} N(t)^2 \mathrm{d}t, \tag{86}$$

with corresponding fitting error

$$\mathrm{Err} = \|N_{\mathrm{dat}}^{375}(t) - N^{375}(t)\|_2^2 + \|N_{\mathrm{dat}}^{750}(t) - N^{750}(t)\|_2^2. \tag{87}$$

Parameter estimation was performed using the *fmincon* function in MATLAB (Mathworks 2015). As in the G-CSF fitting described in Sect. 4.2, the error was evaluated by sampling the functions at one thousand points [with 500 in each time interval because of the scaling in (86)].

Instead of directly fitting the six parameters specified at the start of this section, we let $\tilde{b}_V = b_V / V_{\max}$ and fit to the six parameters μ, b_{N_P}, $V_{\max}$, $\tilde{b}_V$, $\varphi_{N_R}(0)$, and $\varphi_{N_R}^{\mathrm{ratio}}$. This set of parameters is easier to fit to because the constraints (31) and (33) then become simply $\varphi_{N_R}(0) > 0$ and $\tilde{b}_V > G_1^*$, while the original constraints both involve more than one of the unkown parameters.

From (17), (30), and (78), at each step of the optimization the six fitting parameters define the remaining parameters via

$$\begin{aligned} \eta_{N_P}^{\min} &= \mu\, \eta_{N_P}^*, \qquad \varphi_{N_R}^{\max} = \varphi_{N_R}^{\mathrm{ratio}} \varphi_{N_R}^*, \qquad b_V = \tilde{b}_V V_{\max}, \\ \kappa^{\min} &= \theta \kappa^* e^{(\tau_{N_P} \eta_{N_P}^* (1-\mu))}, \qquad b_G = G_{BF}^* \frac{\varphi_{N_R}^{\max} - \varphi_{N_R}(0)}{\varphi_{N_R}^* - \varphi_{N_R}(0)}. \end{aligned} \tag{88}$$

where θ itself is calculated from (85). The Hill coefficient of (8) was set to be $s_1 = 1.5$, midway within its plausible range of values, as explained in Sect. 5.

The estimation of μ requires some caution as its lower bound in (80) changes at each iteration of the optimization as θ varies, and we see from (85) that θ itself depends on three of the parameters to which we are fitting. Nonsensical results are obtained if the model is simulated with μ outside its bounds. Since the constraint is difficult to apply, to ensure that (80) is respected we use a penalty method. Consequently, (80) is checked at each iteration of the optimization and if μ is outside of its bounds μ is reset to the bound and after the simulation is computed Err is multiplied by the penalty factor $e^{|\mu - \mu_{\mathrm{bound}}|^{1/2}}$ which is larger than 1 when $\mu \neq \mu_{\mathrm{bound}}$. The error function thus penalized cannot have a minimum with μ outside of its bounds, and so the optimization routine is forced to find values for μ within the permissible range.

A family of G-CSF kinetic parameter sets is reported in Table 1 in Sect. 4.2. Estimates for the pharmacodynamic parameters were performed for every parameter set in Table 1. The resulting pharmacodynamic parameters are reported in Table 2.

Since G_2^* in the full model (1)–(17) is given by (66) which differs from the value given by (74) for the simplified model (68), (69), the values of G_{prod} and N_{elim} derived for the two models will also be different. In Table 2 the values from Sect. 4.2 for the simplified model are referred to as $N_{\mathrm{elim}}^{\mathrm{simp}}$, and we also state the corresponding value of N_{elim} for the full model from (73) using (67).

Table 2 Parameter estimation results for the pharmacodynamic parameters

Name	Value 1	Value 2	Value 3	Value 4	Value 5	Units
$N_{\text{elim}}^{\text{simp}}$	0.097478	0.6	0.71678	0.8	0.87358	–
N_{elim}	0.3631	0.4508	0.6204	0.7033	0.8153	–
μ	0.96381	0.86303	0.85482	0.84458	0.90768	–
b_{N_P}	0.125	0.026182	0.025994	0.022868	0.024908	ng/mL
$V_{\max}$	7.9932	7.9881	7.9697	7.867	7.994	–
$\tilde{b}_V$	0.031250	0.031251	0.031255	0.031283	0.031261	ng/mL
$\varphi_{N_R}(0)$	0.072801	0.026753	0.023154	0.020056	0.049852	days^{-1}
$\varphi_{N_R}^{\text{ratio}}$	10.9606	11.7257	11.9442	11.3556	11.9706	–
$\eta_{N_P}^{\min}$	1.6045	1.4367	1.4231	1.406	1.5111	days^{-1}
$\varphi_{N_R}^{\max}$	3.9897	4.2682	4.3478	4.1335	4.3574	days^{-1}
b_V	0.24979	0.24964	0.24909	0.24611	0.2499	ng/mL
b_G	6.3999×10^{-5}	0.0002107	0.00019058	0.00018924	0.00018725	–
θ	0.45978	0.18895	0.17099	0.15096	0.32529	–
$\kappa^{\min}$	0.0052359	0.0073325	0.0073325	0.0073325	0.0073325	days^{-1}
Err	0.3482	0.3153	0.2928	0.2843	0.3762	–

$N_{\text{elim}}^{\text{simp}}$ refers to N_{elim} value of the corresponding kinetic parameters for the simplified G-CSF model given in Table 1. N_{elim} is the corresponding value for the full model, then stated are the six fit parameters, followed by the dependent parameters. The approximation error to the data is found by integrating (3) as in (87) and comparing to Wang's data (2001) for a 375- and 750-μg IV infusion of 25 min

It is important to note that if μ were close to 1 and far from its lower bound, then $\kappa^{\min}/\kappa^* \ll 1$, and the wide variation in possible differentiation rates could have potentially destabilizing effects on the stem cells. However, for most of the investigated parameter sets (except for $N_{\text{elim}}^{\text{simp}} = 0.097478$) with the added 'stabilizing' data, μ was found to be essentially equal to its lower bound. In this case $\kappa^{\min}$ is almost equal to κ^*, and the rate of differentiation out of the stem cell compartment is essentially constant and (8) is virtually independent of the influence of G-CSF. For the current model with the imposed stabilizing data, this implies that any change in production is produced by variations in the effective proliferation rate of (9). Without the additional data points, we found parameter estimates where μ was far from its lower bound and $\kappa^{\min}$ was similarly lower than κ^* but these led to unstable dynamics. As shown in Sects. 4.5 and 6, the parameter estimates obtained are shown to successfully reproduce protocols for chemotherapy-alone and chemotherapy with adjuvant G-CSF. Accordingly, differentiation from the hematopoietic stem cells is likely close to constant in reality but from our results, we cannot conclude that differentiation is independent of G-CSF.

Figure 7 shows the comparison of the resulting model solutions for three different values of N_{elim}, two of which are shown to be less optimal. Also included are the corresponding G-CSF predictions without any re-estimation from the values obtained in Sect. 4.2. For $N_{\text{elim}} = 0.097478$, the G-CSF response is well predicted as shown in Fig. 7b, but because of the renal domination of these parameters, the

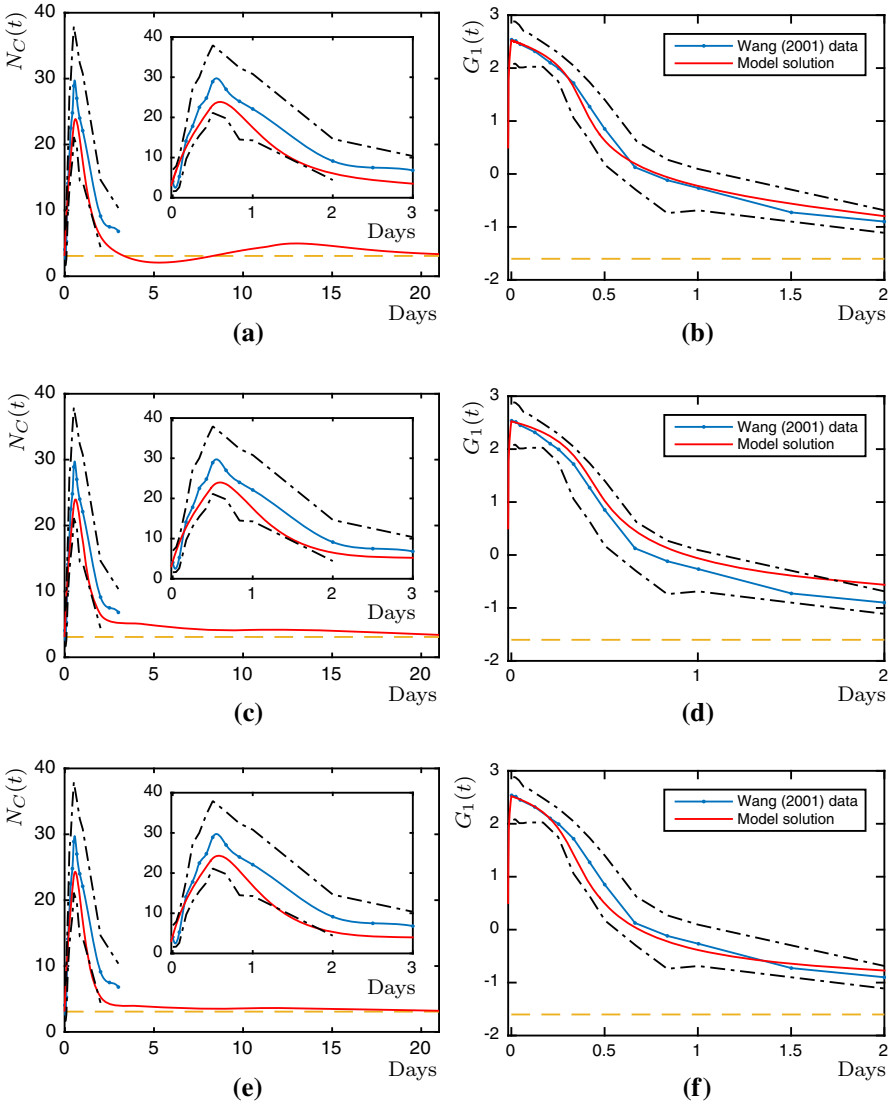

Fig. 7 Simulations of the full model (1)–(17) for various parameter sets with different N_{elim} values. *Left* Circulating neutrophil concentrations in 10^9 cells/L over 21 days, with the first 3 days shown as an *inset*. *Right* The corresponding circulating G-CSF concentrations. *Blue lines with data* digitized data from Fig. 7 (neutrophil concentrations) and Fig. 6 (G-CSF concentrations) of Wang et al. (2001), *red solid lines* model solution, *black dashed lines* maximum and minimum digitized data values from Fig. 7 and Fig. 6 of Wang et al. (2001), *yellow dashed lines* respective homeostatic values. **a** $N_{\text{elim}}^{\text{simp}} = 0.097478$, **b** $N_{\text{elim}}^{\text{simp}} = 0.097478$, **c** $N_{\text{elim}}^{\text{simp}} = 0.80$, **d** $N_{\text{elim}}^{\text{simp}} = 0.80$, **e** $N_{\text{elim}}^{\text{simp}} = 0.87358$ and **f** $N_{\text{elim}}^{\text{simp}} = 0.87358$ (Color figure online)

cytokine paradigm fails in the endogenous-only case. Moreover, repeated administrations of exogenous G-CSF will not accumulate per clinical observations. The G-CSF response seems to be well characterized by the $N_{\text{elim}}^{\text{simp}} = 0.87358$ parameters

in Fig. 7f; however, the dynamics of the neutrophil response in Fig. 7e do not stay within the data bounds, and so are not a good fit. Using $N_{\text{elim}}^{\text{simp}} = 0.8$, both the neutrophil and G-CSF responses are successfully predicted in Fig. 7c, d. The two sets with the lowest errors ($N_{\text{elim}}^{\text{simp}} = 0.71678$ and $N_{\text{elim}}^{\text{simp}} = 0.8$) were used to determine parameters relating to the pharmacodynamic effects of chemotherapy, which is discussed in Sect. 4.5.

4.5 Estimation of Chemotherapy-Related Parameters

To estimate parameters in (38) and (40), data from the results of the Phase I clinical trial of Zalypsis® were digitized from González-Sales et al. (2012). Unlike the data used for fitting in Sects. 4.2 and 4.4, here the protocols differ from one subject to the next and are reported per patient. All dosing regimens were as stated in González-Sales et al. (2012) with doses scaled by body surface area (BSA). Since the subjects were patients undergoing anticancer treatments, deviations from the prescribed protocols were frequent. Thus, only subjects in the top row (A, B) and bottom row (D, E) of Fig. 3 in González-Sales et al. (2012) were retained for our analyses.

As with the parameter estimation of the two previous sections, we define the function $N_{\text{dat}}^{ch_j}(t)$ from a spline fit to the data, where $j = A, B, D, E$ corresponds to each of the retained subjects. Likewise, the function $N^{ch_j}(t)$ was defined from the solution from the DDE solver *ddesd* in MATLAB (Mathworks 2015) for each patient. When the subject was administered two or more cycles of chemotherapy, we took time intervals corresponding to the first two cycles. Thus, the time spans differed for each subject-specific fitting procedure and were: $t_{\text{span}_A} = [0, 43]$, $t_{\text{span}_B} = [0, 41]$, $t_{\text{span}_C} = [0, 47]$, and $t_{\text{span}_D} = [0, 61]$. As explained in Sect. 5, to account for each subject's baseline ANC, we adjust a scaling factor so our homeostasis N^* value matches each individual's. We have previously shown the robustness of a similar model to pharmacokinetic interindividual and interoccasion variability which substantiates this adjustment and the use of average values in physiological models (Craig et al. 2016). For each of the four patients, we define the integrals

$$\|N(t)\|_j^2 = \frac{1}{|t_{\text{span}_j}|} \int_{\min(t_{\text{span}_j})}^{\max(t_{\text{span}_j})} N(t)^2 \mathrm{d}t, \tag{89}$$

where $j = A, B, D, E$. To find average parameter values which fit to all four patients together, we further defined the average error in the L^2 function norm of (89) between the simulated solutions and the data by

$$Err = \frac{1}{4} \sum_j \|N^{ch_j}(t) - N_{\text{dat}}^{ch_j}(t)\|_j^2. \tag{90}$$

Parameters h_Q, $\eta_{N_P}^{\text{inf}}$, s_c, and EC_{50} were then estimated using the *lsqcurvefit* optimization routine in MATLAB (Mathworks 2015) and similarly averaged. These values are reported in Table 3, and the results of Fig. 8 were obtained from simulations using

Table 3 Results of the parameter estimation of chemotherapy effects values

Name	Value 1	Value 2	Units
$N_{\text{elim}}^{\text{simp}}$	0.71678	0.8	–
N_{elim}	0.6204	0.7033	–
h_Q	0.0071122	0.0079657	–
EC_{50}	0.78235	0.72545	ng/mL
s_c	0.90568	0.89816	–
$\eta_{N_P}^{\text{inf}}$	0	0	days^{-1}
Err	0.17068	0.16965	–

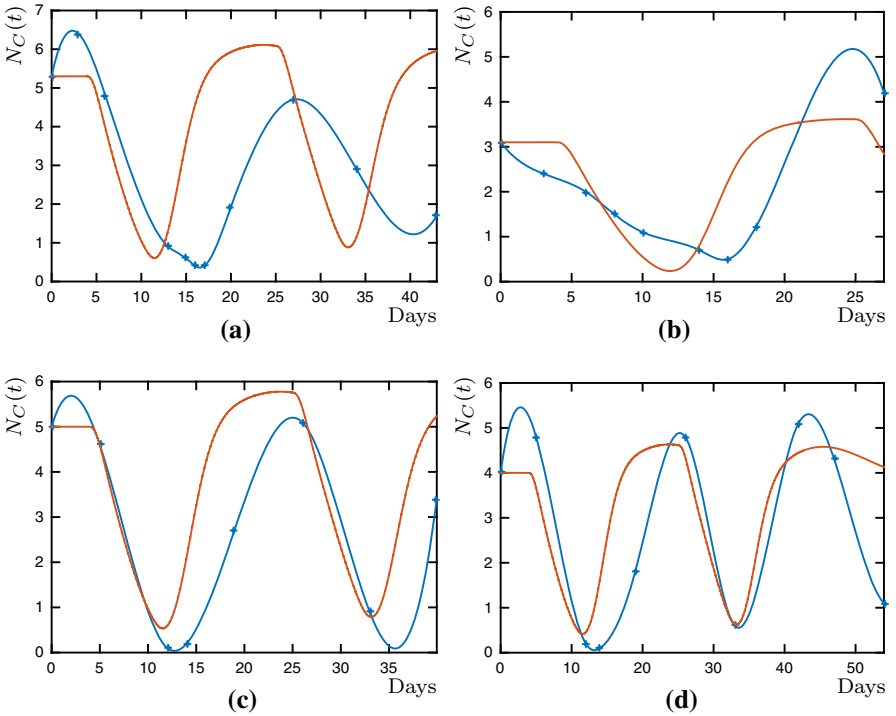

Fig. 8 Results from the chemotherapy parameter fitting for $N_{\text{elim}}^{\text{simp}} = 0.80$ parameters over two chemotherapy cycles. Model solutions were obtained using the parameters given in Table 2 and by simulating the full model (1)–(17). Chemotherapeutic concentrations are obtained via (37) and (40). Equation (18) is replaced by (38) and solved by using (39). Data and experimental protocols from Fig. 3 of González-Sales et al. (2012). *Blue lines with data* digitized data, *red solid lines* model solution. **a** Subject A. **b** Subject B. **c** Subject D. **d** Subject E (Color figure online)

these parameters. For each of h_Q, EC_{50}, s_c, and $\eta_{N_P}^{\text{inf}}$, similar estimates were obtained for $N_{\text{elim}}^{\text{simp}} = 0.71578$ and $N_{\text{elim}}^{\text{simp}} = 0.8$, although the average error of $N_{\text{elim}}^{\text{simp}} = 0.8$ is slightly smaller and was accordingly retained as optimal.

5 Parameter Values

Here we summarize the parameter values we use in the full model taken from experimental results and the fitting procedures described in Sect. 4. For the model to be self-consistent these parameters must be positive and satisfy the parameter constraints that we derived above, namely (30), (31), (33), (59), (60), and (80).

The main model parameters are stated in Table 4. For the stem cells we reuse parameter values for Q^*, γ_Q, τ_Q, f_Q, s_2 and $\beta(Q^*)$ from previous modelling (sometimes rounding them to fewer significant figures). The value of θ_2 is obtained by evaluating (6) at homeostasis and rearranging to obtain

$$\theta_2 = \left[\frac{(Q^*)^{s_2}\beta(Q^*)}{f_Q - \beta(Q^*)}\right]^{\frac{1}{s_2}}. \tag{91}$$

In Table 4 we quote a value of θ_2 to five significant figures, but in our computations all parameters defined by formulae are evaluated to full machine precision. This ensures that our differential equation model has a steady state exactly at the stated homeostasis values.

For the neutrophil parameters we mainly take experimental values from the work of Dancey et al. (1976) and use the formulae of Sect. 4.1 to determine the related model parameter values. However, some choices and adjustments need to be made to ensure that the values are consistent with the model. Dancey et al. (1976) measured the circulating neutrophil pool to be 0.22×10^9 cells/kg and the recovery rate to be 0.585 from which we obtain the total blood neutrophil pool N^* (including the marginated pool) to be

$$N^* = \frac{0.22}{0.585} \approx 0.3761 \times 10^9 \text{ cells/kg}. \tag{92}$$

Since $N(t)$ measures the total blood neutrophil pool in units of 10^9 cells/kg some care needs to be taken when comparing to data, where absolute neutrophil counts (ANC) measure the circulating neutrophil pool in units of cells/μL. Based on 70 kg of body mass and 5 L of blood we have the default conversion factor for healthy subjects of

$$ANC = 0.585 \times \frac{70}{5} \times 1000 \times N(t) = 8190\, N(t) \text{ cells/μL}. \tag{93}$$

This gives a baseline homeostasis ANC of $8190N^* = 3080$ cells/μL, well within the accepted normal range of 1800–7000 cells/μL (Ryan 2016). When comparing our model to data for individuals with different baseline ANCs (as in Sect. 4.5) we adjust the conversion factor (93), but not the parameter values in our model, so that N^* gives the homeostasis ANC of the data.

Dancey et al. (1976) measures the proliferation and maturation phases at homeostasis to be $N_P^* = 2.11 \times 10^9$ cells/kg (mainly promyelocytes and myelocytes) and $N_M^* = 3.33 \times 10^9$ cells/kg (metamyelocytes and bands). Using these numbers in the calculations in Sect. 4.1 results in a proliferation time τ_{N_P} defined by (64) of about

Table 4 Model parameters

Name	Interpretation	Value	Units	Source
γ_Q	HSC apoptosis rate	0.1	days^{-1}	Brooks et al. (2012) and Craig et al. (2015)
τ_Q	Time for HSC reentry	2.8	days	Mackey (2001), Bernard et al. (2003), Lei and Mackey (2011), and Craig et al. (2015)
A_Q^*	HSC amplification factor	1.5116[a]	–	Eq. (7)
f_Q	Maximal HSC reentry rate	8	days^{-1}	Bernard et al. (2003), Brooks et al. (2012), and Craig et al. (2015)
s_2	HSC reentry Hill coefficient	2	–	Bernard et al. (2003), Brooks et al. (2012), and Craig et al. (2015)
θ_2	Half-effect HSC concentration	0.080863[a]	10^6 cells/kg	Eq. (91)
κ_δ	HSC differentiation rate to other lines	0.014665[a]	days^{-1}	Eq. (45)
$\kappa^{\min}$	HSC-neutrophil minimal differentiation rate	0.0073325[a]	days^{-1}	Eq. (88)
κ^*	HSC-neutrophil homeodifferentiation rate	0.0073325[a]	days^{-1}	Eq. (45)
s_1	HSC-neutrophil differentiation Hill coefficient	1.5	–	Eq. (96)
$\eta_{N_P}^*$	Neutrophil homeostasis effective proliferation rate	1.6647[a]	days^{-1}	Eq. (63)
b_{N_P}	Neutrophil proliferation M-M constant	0.022868	ng/mL	Fit Table 2
$\eta_{N_P}^{\min}$	Neutrophil minimal proliferation rate	1.4060	days^{-1}	Eq. (88)
τ_{N_P}	Neutrophil proliferation time	7.3074[a]	days	Eq. (64)
$V_{\max}$	Maximal neutrophil maturation velocity	7.8670	–	Fit Table 2
b_V	Maturation velocity half-effect concentration	0.24611	ng/mL	Eq. (88)

Table 4 continued

Name	Interpretation	Value	Units	Source
a_{N_M}	Homeostasis neutrophil maturation time	3.9	days	Dancey et al. (1976), Hearn et al. (1998) and (95)
γ_{N_M}	Neutrophil death rate in maturation	0.15769[a]	days^{-1}	Eq. (57)
$\varphi^*_{N_R}$	Homeostasis reservoir release rate	0.36400[a]	days^{-1}	Eq. (52)
$\varphi^{\max}_{N_R}$	Maximal reservoir release rate	4.1335[a]	days^{-1}	Eq. (88)
b_G	Reservoir release half-effect concentration	1.8924×10^{-4}	–	Eq. (88)
γ_{N_R}	Neutrophil death rate in reservoir	0.0063661[a]	days^{-1}	Eq. (54)
γ_N	Neutrophil removal rate from circulation	35/16	days^{-1}	Eq. (51)
G^*_1	Homeostasis free G-CSF concentration	0.025	ng/mL	Watari et al. (1989), Kawakami et al. (1990), Barreda et al. (2004) and Krzyzanski et al. (2010)
G^*_{BF}	Homeostasis neutrophil receptor bound fraction	1.5823×10^{-5}	–	Eq. (16)
G_{prod}	Endogenous G-CSF production rate	0.014161[a]	ng/mL/day	Eq. (67)
V	Bound G-CSF conversion factor	0.525	$\frac{\text{ng/mL}}{10^9\ \text{cells/kg}}$	Eq. (65)
k_{ren}	G-CSF renal elimination rate	0.16139	days^{-1}	Fit Table 1
k_{int}	G-CSF effective internalization rate	462.42	days^{-1}	Fit Table 1
k_{12}	G-CSF receptor binding coefficient	2.2423	$(\text{ng/mL})^{-\text{Pow}}\ \text{days}^{-1}$	Fit Table 1
k_{21}	G-CSF receptor unbinding rate	184.87	days^{-1}	Fit Table 1
Pow	Effective G-CSF binding coefficient	1.4608	–	Fit Table 1

[a] These parameters are displayed to five significant figures here, but the value is actually defined by the stated equation, and in simulations/computations we use the stated formula to define the value to machine precision

26 days. In our model τ_{N_P} is the time from when the HSC first commits to differentiate to the neutrophil line to the end of proliferation of the neutrophil precursors. Although this time has never been definitively measured, 26 days seems to be too long. This is confirmed by the time to neutrophil replenishment in the blood after both allogenic and autologous stem cell transplantation (Baiocci et al. 1993; Cairo et al. 1992), where circulating neutrophils are seen 2 weeks after the transplant. We suspect that this overly long proliferation time results from the simplification in our model of considering proliferation as a single homogenous process as detailed in Sect. 3.3.

To obtain a more realistic proliferation time of around a week, close to the 6.3 days that Smith (2016) states, we keep the total of $N_P^* + N_M^* = 5.44 \times 10^9$ cells/kg as found by Dancey et al. (1976), but redistribute cells between proliferation and maturation and set

$$N_P^* = 0.93 \times 10^9 \text{ cells/kg}, \quad N_M^* = 4.51 \times 10^9 \text{ cells/kg}. \tag{94}$$

Dancey et al. (1976) measured the half-removal time of neutrophils from circulation to be $t_{1/2} = 7.6$ h. Accordingly, using (51) and rounding, we set $\gamma_N = 35/16 = 2.1875$ days^{-1} and obtain $\tau_{N_C}^*$ as the reciprocal of this. Then Eq. (58) imposes the constraint that $a_{N_M} < 5.4823$ days. If we set $a_{N_M} = 3.9$ days close to the value of 3.8 days found by Hearn et al. (1998), then (60) imposes the constraint that $\tau_{N_R}^* \in (1.9543, 2.7472)$. Hence, we take

$$a_{N_M} = 3.9 \text{ days}, \quad \tau_{N_R}^* = 2.7 \text{ days}, \tag{95}$$

so that both constraints are satisfied, and $a_{N_M} + \tau_{N_R}^* = 6.6$ days, the value given in Dancey et al. (1976). The rest of the neutrophil homeostasis parameters are calculated using the formulae of Sect. 4.1, paying attention in (61) to multiply Q^* by 10^{-3} to convert it to the same units as N_R^*.

The G-CSF pharmacokinetic parameters are fit using the simplified G-CSF model (68), (69) as described in Sect. 4.2. This produces multiple, but equally plausible, parameter sets but as described in previous sections not all of these result in good fits to data when we consider the neutrophil response of the full model (1)–(17) to administrations of G-CSF or of chemotherapy. Consequently as stated in Sect. 4.5, to obtain the best responses of the system to these scenarios we use the fourth set of pharmacokinetic parameters from Table 1 which for the simplified G-CSF model have $N_{\text{elim}}^{\text{simp}} = 0.8$ to define k_{ren}, k_{12}, k_{21}, k_{int}, and Pow, as well as the exogenous G-CSF parameters V_d, F, k_a (where the last three are dose dependent). Equations (66), (67), and (73) then define G_2^*, G_{prod}, and $N_{\text{elim}} = 0.7033$ for the full model.

At G-CSF knockout, from Bugl et al. (2012), Lui et al. (2013) we have $C_{ko} \in [0.2, 0.3]$, so it is natural to set $C_{ko} = 0.25$.

For the pharmacodynamic parameters, similar to Pow, arguments could be made for choosing $s_1 = 1$ or $s_1 = 2$, but having fit Pow and finding it close to 1.5, we will simply set

$$s_1 = 1.5 \tag{96}$$

to reduce the number of parameters that need to be fit by one. The remaining pharmacodynamic parameters μ, b_{N_P}, $V_{\max}$, $\tilde{b}_V$, $\varphi_{N_R}(0)$, and $\varphi_{N_R}^{\text{ratio}}$ were then fit as described in Sect. 4.4, with these parameters defining values of the dependent parameters $\eta_{N_P}^{\min}$, $\varphi_{N_R}^{\max}$, b_V, and b_G via (88). From Sect. 4.3 we also obtain values for θ from (85) and $\kappa^{\min}$ from (88). Each set of kinetic parameters from Table 1 defines a different set of pharmacodynamic parameters as reported in Table 2, but as noted already we prefer the parameter set for $N_{\text{elim}}^{\text{simp}} = 0.80$ which corresponds to $N_{\text{elim}} = 0.7033$.

The full set of parameter values for our combined neutrophil and G-CSF model (1)–(17) are given in Table 4, along with their units, interpretation, and source. Since some of these parameters are defined by equations involving auxiliary parameters that do not explicitly appear in the full model we state these parameters and their source in Table 5. Parameters related to the pharmacokinetics and pharmacodynamics of both of the exogenous drugs which have not previously been stated are given in Table 6.

6 Model Evaluation and Functional Responses

One of the major successes of this study rests in its translational nature and, by extension, its relevance for clinicians and physiologists. Anticancer treatments frequently result in myelosuppression (neutropenia, or low neutrophil counts), and this has significant consequences on patients' treatment protocols and, ultimately, the therapeutic outcome. Accordingly, one of our main interests is in application to G-CSF dose adaptation during chemotherapy. Having estimated the G-CSF pharmacokinetic, homeostasis related, and chemotherapy pharmacodynamic parameters individually as described in Sects. 4.2, 4.4, and 4.5, a convincing demonstration of the robustness of the model is its ability to successfully predict drug–drug interaction scenarios. Therefore, we will compare the model's predictions of the concurrent administration of anticancer drugs with adjuvant G-CSF support to clinical data to evince the clinical applicability of our model. We previously studied G-CSF treatment adaptation in a model with simplified G-CSF kinetics and pharmacodynamics (Craig et al. 2015). The current model provides for more realistic predictions than in our previous work (Craig et al. 2015).

Therefore, as in Craig et al. (2015), we simulated the CHOP14 protocol described in Pfreundschuh et al. (2004b) and Pfreundschuh et al. (2004a) which includes the administration of both chemotherapy and exogenous G-CSF. Although the chemotherapeutic drug modelled in Sect. 3.5 is not part of the combination therapy of the CHOP14 regimen, the cytotoxic effects of the anticancer drugs are presumed to be similar. To compare to the CHOP14 data published in Krinner et al. (2013), we simulated a regimen of six cycles of 14-day periodic chemotherapeutic treatment with rhG-CSF treatment beginning 4 days after the administration of chemotherapy and continuing for ten administrations per cycle. As in Craig et al. (2015), the simulated dose of 4 μg of Zalypsis® was selected from the optimal regimens identified in González-Sales et al. (2012) and per the CHOP14 protocol outlined in Pfreundschuh et al. (2004b), Pfreundschuh et al. (2004a), ten 300-μg doses of subcutaneous G-CSF were simulated per cycle. The lower dose of 300 μg was selected since we assumed an average weight of 70 kg per patient throughout.

Table 5 Auxiliary parameters which are not in the model in Sect. 2, but whose values are used to define other parameters

Name	Interpretation	Value	Units	Source
Q^*	HSC homeostasis concentration	1.1	10^6 cells/kg	Bernard et al. (2003), Lei and Mackey (2011), and Craig et al. (2015)
$\beta(Q^*)$	HSC reentry rate	0.043	days^{-1}	Mackey (2001) and Craig et al. (2015)
N^*	Homeostasis total blood neutrophil pool (TBNP)	0.22/0.585	10^9 cells/kg	Eq. (92)
N_R^*	Homeostasis neutrophil reservoir concentration	2.26	10^9 cells/kg	Dancey et al. (1976)
N_P^*	Homeostasis neutrophil proliferation concentration	0.93	10^9 cells/kg	Eq. (94)
N_M^*	Homeostasis neutrophil maturation concentration	4.51	10^9 cells/kg	Eq. (94)
G_2^*	Homeostasis bound G-CSF concentration	2.1899×10^{-5}	ng/mL	Eq. (66)
$\tau_{N_R}^*$	Homoeostasis neutrophil mean time in reservoir	2.7	days	Dancey et al. (1976), Hearn et al. (1998) and (95)
$\tau_{N_C}^*$	Homoeostasis neutrophil mean time in circulation	16/35	days	Dancey et al. (1976)
$\tau_{1/2}$	Circulating neutrophil half-removal time	7.6	h	Dancey et al. (1976)
A_N^*	Homeostasis neutrophil proliferation+maturation amplification	1.0378×10^5[a]	–	Eq. (61)
$\tilde{b}_V$	Scaled maturation half-effect concentration	0.031283	ng/mL	Fit Table 2
$\varphi_{N_R}^{\text{ratio}}$	Ratio of maximal and homeostasis reservoir release rates	11.356	–	Fit Table 2
$\varphi_{N_R}(0)$	Minimal reservoir release rate	0.020056	days^{-1}	Fit Table 2
θ	Ratio of rate cells leave proliferation at knockout to homeostasis	0.15096	–	Eq. (85)
C_{ko}	Knockout total blood neutrophil pool fraction	0.25	–	Bugl et al. (2012) and Lui et al. (2013)
μ	Ratio of minimal and homeostasis proliferation rates	0.84458	–	Fit Table 2

[a] These parameters are displayed to five significant figures here, but the value is actually defined by the stated equation, and in simulations/computations we use the stated formula to define the value to machine precision

Table 6 Exogenous drug administration parameters determined by parameter fitting as explained in Sects. 4.2 and 4.5

Name	Interpretation	Value	Units	Source
Filgrastim				
300 mcg dose				
V_d	Volume of distribution	4754.7	mL	Fit Table 1
F	Bioavailable fraction	0.64466	–	Fit Table 1
k_a	Subcutaneous rate of absorption	8.0236	days^{-1}	Fit Table 1
375 mcg dose				
V_d	Volume of distribution	2322.9	mL	Fit Table 1
F	Bioavailable fraction	0.49964	–	Fit Table 1
k_a	Subcutaneous rate of absorption	6.6133	days^{-1}	Fit Table 1
750 mcg dose				
V_d	Volume of distribution	2178.0	mL	Fit Table 1
F	Bioavailable fraction	0.75	–	Fit Table 1
k_a	Subcutaneous rate of absorption	5.143	days^{-1}	Fit Table 1
Zalypsis®				
k_{fp}	Rate of exchange from compartment f to p	18.222	days^{-1}	Pérez-Ruixo et al. (2012)
$k_{sl_1 p}$	Rate of exchange from compartment sl_1 to p	0.6990	days^{-1}	Pérez-Ruixo et al. (2012)
k_{pf}	Rate of exchange from compartment p to f	90.2752	days^{-1}	Pérez-Ruixo et al. (2012)
k_{psl_1}	Rate of exchange from compartment p to sl_1	8.2936	days^{-1}	Pérez-Ruixo et al. (2012)
k_{el_C}	Rate of elimination	132.0734	days^{-1}	Pérez-Ruixo et al. (2012)
$k_{sl_2 f}$	Rate of exchange from compartment sl_2 to f	62.5607	days^{-1}	Pérez-Ruixo et al. (2012)
k_{fsl_2}	Rate of exchange from compartment f to sl_2	9.2296	days^{-1}	Pérez-Ruixo et al. (2012)
BSA	Body surface area	1.723	m^2	Pérez-Ruixo et al. (2012)

Table 6 continued

Name	Interpretation	Value	Units	Source
h_Q	Effect of chemotherapy on $Q(t)$	0.0079657	–	Fit Table 3
EC_{50}	Half-maximal effect of chemotherapy on η_{N_P}	0.75390	–	Fit Table 3
s_c	Chemotherapy effect Hill coefficient	0.89816	–	Fit Table 3
$\eta_{N_P}^{\inf}$	Proliferation rate with infinite chemotherapy dose	0	days^{-1}	Fit Table 3

For Zalpysis®, p, plasma/central compartment; f, fast-exchange tissues; sl_1, first slow-exchange tissues; sl_2, second slow-exchange tissues

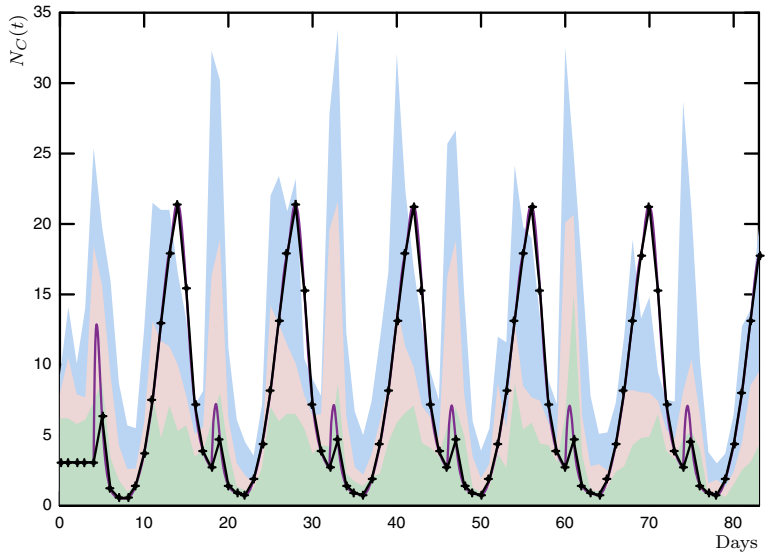

Fig. 9 Comparison of the predicted neutrophil response to the CHOP14 protocol Pfreundschuh et al. (2004b) and Pfreundschuh et al. (2004a) for $N_{\text{elim}}^{\text{simp}} = 0.80$. In this regimen, 4 μg of Zalypsis® given by a 1-h IV infusion is administered 14 days apart, beginning on day 0, for 6 cycles (84 days total). Per cycle, 10 administrations of 300-μg subcutaneous doses of filgrastim are given beginning 4 days after the start of the chemotherapeutic cycle and continuing to day 13 post-chemotherapy. The simulation is compared to data from Krinner et al. (2013), presented in quartiles. *In pale green* the first quartile, *in pale pink* median range, *in pale blue* third quartile. *Black line with sampling points* model prediction sampled every day at clinical sampling points, *solid purple line* full model prediction (Color figure online)

Figure 9 shows the result of the neutrophil response comparison of the model's prediction to the clinical data. Unlike experimental settings where information on the HSCs, the marrow neutrophils, and the bound G-CSF concentrations are unavailable, the model's solutions for $Q(t)$, $N_R(t)$, and $G_2(t)$ are easily obtainable and provide insight into not only the mechanisms responsible for myelosuppresion during chemotherapy, but also ways in which this toxicity might be avoided. Identifying specific mechanisms impacting the appearance of neutropenia during chemotherapy has important ramifications for clinicians (who can then better predict the onset of myelosuppression) and is a further example of the translational nature of physiological models such as the one reported here. In Fig. 10, the HSCs, neutrophils in the marrow reservoir, and bound and unbound G-CSF are all seen to converge to periodic responses. However, while the reduction in HSC concentrations is minimal (Fig. 10a) the neutrophil marrow reservoir is shown in Fig. 10b to become severely depleted. This depletion is caused by the delayed effects of the administration of chemotherapy but also the rapid transit of cells from the reservoir into the blood caused by the introduction of exogenous G-CSF 4 days post-chemotherapy (see Fig. 11e below). This in turn prevents ANC recoveries from depressed values, despite the administration of G-CSF. As in Vainstein et al. (2005) and Craig et al. (2015), it is likely that delaying the beginning of prophylactic G-CSF support during chemotherapy would help to combat myelosuppresion, but this is a future avenue of investigation.

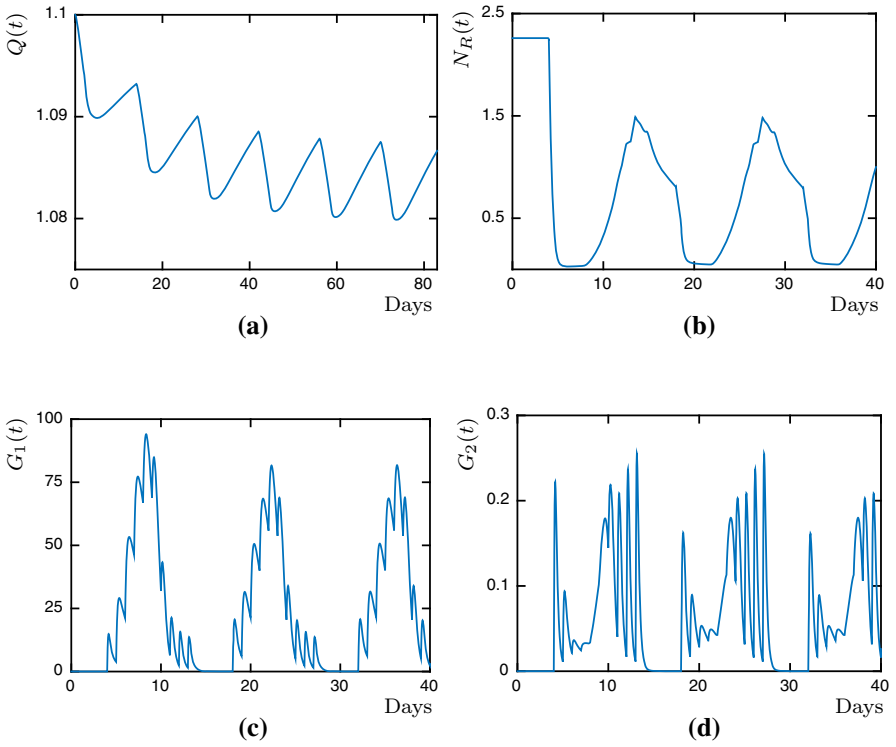

Fig. 10 Model responses to the CHOP14 protocol as described in Sect. 6. **a** $Q(t)$ over the six CHOP cycles detailed above, **b–d** $N_R(t)$, $G_1(t)$, and $G_2(t)$ over three CHOP cycles

It is also revealing to study how each of the model's functions correspond to the estimated parameters to gain further insight on the mechanisms of granulopoiesis. Figure 11 shows the functions $\kappa(G_1)$, $\eta_{N_P}(G_1)$, $\eta_{N_P}^{\text{chemo}}(G_1)$, $V_{N_M}(G_1)$, and $\varphi_{N_R}(G_{BF})$ and identifies their respective homeostatic levels. We can see that $\varphi_{N_R}(G_{BF})$ in Fig. 11e has a homeostasis concentration $\varphi_{N_R}(G_{BF}^*)$ very close to $\varphi_{N_R}(0)$. This reflects the ability of the granulopoietic system to respond rapidly in the case of emergencies (Rankin 2010) but also supports the hypothesis that early prophylactic support with G-CSF during chemotherapy may hasten the emptying of the reservoir due to the responsiveness of $\varphi_{N_R}(G_{BF}(t))$ in particular (Craig et al. 2015; Vainas et al. 2012).

7 Discussion

Clinically relevant translational models in medicine not only must accurately depict different and independent treatment regimes (Vainstein et al. 2005), but must also be able to reconstruct homeostatic and pathological cases which may be intervention independent. The granulopoiesis model we have developed is physiologically relevant and, perhaps most importantly, provides insight beyond that which is clinically measurable. The updated pharmacokinetic model of G-CSF, novel in that it explicitly accounts for

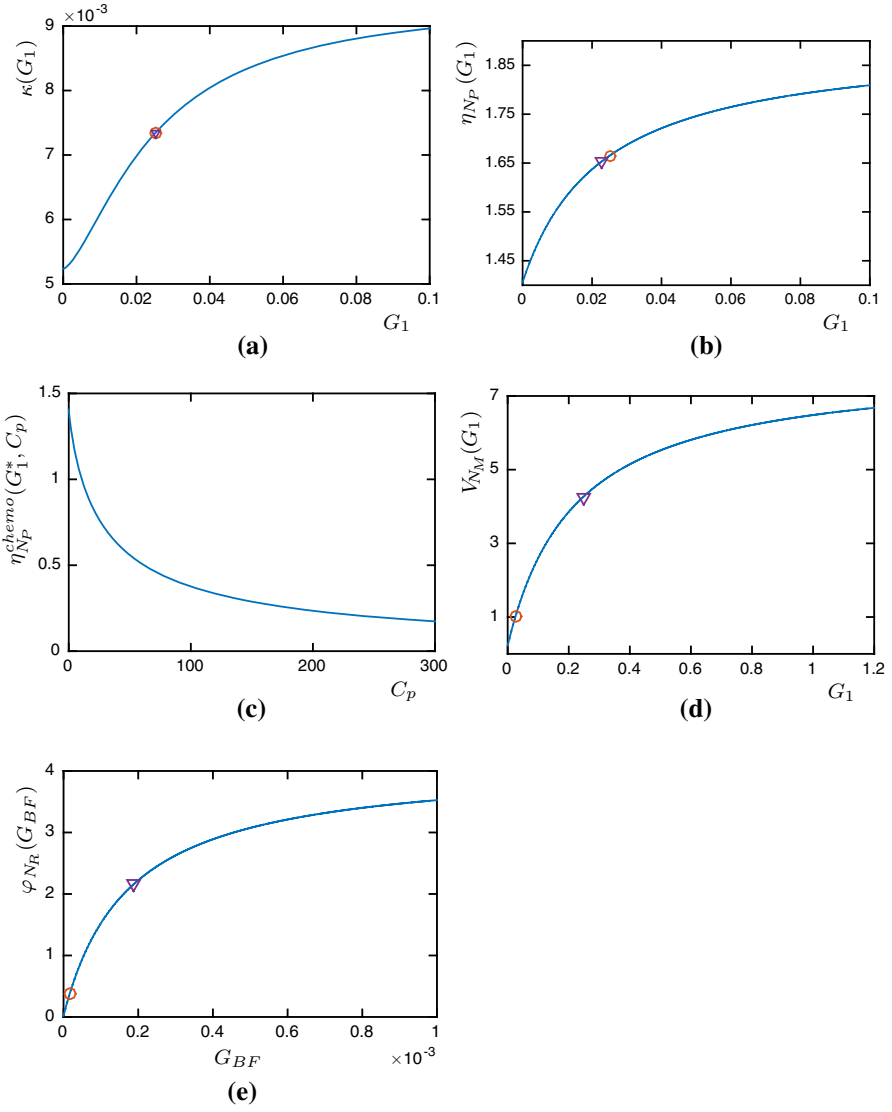

Fig. 11 Visualization of the granulopoiesis model's mechanisms as functions of their variables (*solid blue lines*) with their respective homeostatic (*red circles*) and half-effect values (*purple triangles*), when relevant (Color figure online)

unbound and bound concentrations, correctly accounts for G-CSF dynamics whereas previous one compartment models all resulted in renal dominated dynamics. The new pharmacokinetic model also further allows us to comment on the principal mechanisms driving the production of neutrophils. Although the relatively small number of neutrophil progenitors do not have a significant effect on G-CSF kinetics, our results suggest that differentiation, proliferation, and maturation speed are driven primarily by signalling from G-CSF bound to neutrophil progenitors, and not from signalling of G-CSF bound to mature neutrophils. We can further characterize the principal processes

governing myelosuppression during the concurrent administration of chemotherapy and prophylactic G-CSF, which we have determined lies in the simultaneous depletion of the marrow reservoir by high doses of exogenous G-CSF combined with fewer neutrophils reaching the reservoir due to the cytotoxicity of the anticancer drug.

The modelling reported here combines a number of original approaches to the conceptualization of physiological, pharmacokinetic, and pharmacodynamics models and to the estimation of parameters and model verification. For example, traditional least squares estimation was redefined using functions which ensured robustness and allowed for comparisons of predictions to data over richly sampled intervals instead of at fewer data points. Moreover, the model's physiological realism served as a means of evaluating the suitability of optimized parameter values so we were not relying solely on goodness-of-fit, which can obfuscate the biological relevance of results (van der Graaf and Benson 2011). The inclusion of the detailed characterizations of physiological mechanisms in our model therefore serves as a litmus test of suitability in addition to providing intuition about the processes driving granulopoiesis.

The broader implications of the approaches outlined in this work extend into various domains. The derivation of a delay differential equation model with variable aging rate from an age-structured PDE, as described in Sect. 3.3, is mathematically significant and its intricate nature has led to previous modelling errors. As mentioned, the fitting procedures outlined in Sects. 4.2, 4.4, and 4.5 motivate the development of more refined least squares methods and parameter estimation techniques. Additionally, the novel pharmacokinetic model of G-CSF has ramifications with respect to the usual approaches used by PK/PD modellers. The mischaracterization of the elimination dynamics, despite the inclusion of internalization terms, has led to models which contradict what is known of the physiology. While they can characterize certain clinical situations, like the single administration of exogenous G-CSF, they fail when applied to more complex scenarios. Without accounting for the entire process of neutrophil development or using physiological rationale for a model's parameters, one is unable to judge whether a model captures the complicated dynamics of granulopoiesis. In the model we have developed, we have ensured the accuracy of its predictions and the appropriateness of its parameters through careful construction. In turn, this rational approach has implications for the clinical practice where it can serve to optimize dosing regimens in oncological settings and also serve to pinpoint the origins of dynamical neutrophil disorders like cyclic neutropenia, ultimately contributing to the improvement of patient care and outcomes.

Acknowledgments A.R.H. and M.C.M. are grateful to the National Science and Engineering Research Council (NSERC), Canada, for funding through the Discovery Grant program. M.C. wishes to thank NSERC for funding from the PGS-D program. We are grateful to Fahima Nekka, Jun Li, Jacques Bélair, and David Dale for their insight and support. We would also like to thank both anonymous reviewers for their helpful and insightful comments.

References

Baiocci G, Scambia G, Benedetti P, Menichella G, Testa U, Pierelli L, Martucci R, Foddai ML, Bizzi B, Mancuso S, Peschle C (1993) Autologous stem cell transplantation: sequential production of hematopoietic cytokines underlying granulocyte recovery. Cancer Res 53:1297–1303

Barreda DR, Hanington PC, Belosevic M (2004) Regulation of myeloid development and function by colony stimulating factors. Dev Comp Immunol 28(5):509–554
Basu S, Hodgson G, Katz M, Dunn AR (2002) Evaluation of role of G-CSF in the production, survival, and release of neutrophils from bone marrow into circulation. Blood 100:854–861
Bernard S, Bélair J, Mackey MC (2003) Oscillations in cyclical neutropenia: new evidence based on mathematical modeling. J Theor Biol 223:283–298
Brooks G, Langlois GP, Lei J, Mackey MC (2012) Neutrophil dynamics after chemotherapy and G-CSF: the role of pharmacokinetics in shaping the response. J Theor Biol 315:97–109
Bugl S, Wirths S, Müller MR, Radsak MP (2012) Current insights into neutrophil homeostasis. Ann N Y Acad Sci 1266:171–178
Cairo MS, Suen Y, Sender L, Gillan ER, Ho W, Plunkett JM, van de Ven C (1992) Circulating granulocyte colony-stimulating factor (G-CSF) levels after allogenic and autologous bone marrow transplantation: endogenous G-CSF production correlates with myeloid engraftment. Blood 79:1869–1873
Colijn C, Mackey MC (2005a) A mathematical model of hematopoiesis: I. Periodic chronic mylogenous leukemia. J Theor Biol 237:117–132
Colijn C, Mackey MC (2005b) A mathematical model of hematopoiesis: II. Cyclical neutropenia. J Theor Biol 237:133–146
Craig M, González-Sales M, Li J, Nekka F (2016) Impact of pharmacokinetic variability on a mechanistic physiological pharmacokinetic/pharmacodynamic model: a case study of neutrophil development, PM00104, and filgrastim. In: Toni B (ed) Mathematical sciences with multidisciplinary applications, Springer Proceedings in Mathematics and Statistics. Springer Science + Business Media, New York, ISBN 978-3-319-31323-8
Craig M, Humphries AR, Bélair J, Li J, Nekka F, Mackey MC (2015) Neutrophil dynamics during concurrent chemotherapy and G-CSF administration: mathematical modelling guides dose optimisation to minimise neutropenia. J Theor Biol 385:77–89
Dale DC, Mackey MC (2015) Understanding, treating and avoiding hematological disease: better medicine through mathematics? Bull Math Biol 77:739–757
Dale DC, Welte K (2011) Hematopoietic growth factors in oncology. Springer, Heidelberg
Dancey JT, Deubelbeiss KA, Harker LA, Finch CA (1976) Neutrophil kinetics in man. J Clin Investig 58:705–715
DiPiro JT, Spruill WJ, Wade WE, Blouin RA, Pruemer JM (eds) (2010) Concepts in clinical pharmacokinetics, vol 5. American Society of Health-System Pharmacists, Bethesda
Durand C, Charbord P (2010) Stem cell biology and regenerative medicine, vol 3. River Publishers, Aalborg
Endele M, Etzrodt M, Schroeder T (2014) Instruction of hematopoietic lineage choice by cytokine signaling. Exp Cell Res 329:207–213
Foley C, Bernard S, Mackey MC (2006) Cost-effective G-CSF therapy strategies for cyclical neutropenia: mathematical modelling based hypotheses. J Theor Biol 238:756–763
Foley C, Mackey MC (2009a) Dynamic hematological disease: review. J Math Biol 58:285–322
Foley C, Mackey MC (2009b) Mathematical model for G-CSF administration after chemotherapy. J Theor Biol 257:27–44
Friberg LE, Karlsson MO (2003) Mechanistic models for myelosuppression. Invest New Drugs 21:183–194
González-Sales M, Valenzuela B, Pérez-Ruixo C, Fernández Teruel C, Miguel-Lillo B, Soto Matos A et al (2012) Population pharmacokinetic-pharmacodynamic analysis of neutropenia in cancer patients receiving PM00104 (Zalypsis®). Clin Pharmacokinet 51:751–764
Greeenbaum AM, Link DC (2011) Mechanisms of G-CSF-mediated hematopoietic stem and progenitor mobilization. Leukemia 25:211–217
Hammond WP, Csiba E, Canin A, Hockman H, Souza LM, Layton JE, Dale DC (1991) Chronic neutropenia. A new canine model induced by human granulocyte colony-stimulating factor. J Clin Investig 87(2):704–710
Hearn T, Haurie C, Mackey MC (1998) Cyclical neutropenia and the peripherial control of white blood cell production. J Theor Biol 192:167–181
Kawakami M, Tsutsumi H, Kumakawa T, Abe H, Hirai M, Kurosawa S, Mori M, Fukushima M (1990) Levels of serum granulocyte colony-stimulating factor in patients with infections. Blood 76(10):1962–1964
Kazarinoff ND, van den Driessche P (1979) Control of oscillations in hematopoiesis. Science 203:1348–1350
King-Smith EA, Morley A (1970) Computer simulation of granulopoiesis: normal and impaired granulopoiesis. Blood 36:254–262

Krinner A, Roeder I, Loeffler M, Scholz M (2013) Merging concepts—coupling an agent-based model of hematopoietic stem cells with an ODE model of granulopoiesis. BMC Syst Biol 7:117
Krzyzanski W, Wiczling P, Lowe P, Pigeolet E, Fink M, Berghout A, Balser S (2010) Population modeling of filgrastim PK-PD in healthy adults following intravenous and subcutaneous administrations. J Clin Pharmacol 9(Suppl):101S–112S
Kuwabara T, Kato Y, Kobayashi S, Suzuki H, Sugiyama Y (1994) Nonlinear pharmacokinetics of a recombinant human granulocyte colony-stimulating factor derivative (Nartograstim): species differences among rats, monkeys and humans. J Pharmacol Exp Ther 271:1535–1543
Layton JE, Hall NE (2006) The interaction of G-CSF with its receptor. Front Biosci 31:177–199
Lei J, Mackey MC (2011) Multistability in an age-structured model of hematopoiesis: cyclical neutropenia. J Theor Biol 270:143–153
Lui G, Yang H, Wang X, Chu Y (2013) Modulation of neutrophil development and homeostasis. Curr Mol Med 13:1270–1283
Mackey MC (2001) Cell kinetic status of hematopoietic stem cells. Cell Prolif 34:71–83
Mackey MC, Aprikyan AAG, Dale DC (2003) The rate of apoptosis in post mitotic neutrophil precursors of normal and neutropenic humans. Cell Prolif 36:27–34
Maholtra V, Perry MC (2003) Models of anti-cancer therapy. Classical chemotherapy: mechanism, toxicities, and the therapeutic window. Cancer Biol Ther 2:S2–S4
Mathworks (2015) MATLAB 2015a. Mathworks, Natick
Molineux G (2011) Granulocyte colony-stimulating factors. In: Lyman GH, Dale DC (eds) Hematopoietic growth factors in oncology. Springer Science + Business Media, New York
Molineux G, Arvedson T, Foote M (2012) Twenty years of G-CSF clinical and nonclinical discoveries. Springer Basel AG, Basel
Pérez-Ruixo C, Valenzuela B, Fernández Teruel C, González-Sales M, Miguel-Lillo B, Soto-Matos A et al (2012) Population pharmacokinetics of PM00104 (Zalypsis®) in cancer patients. Cancer Chemother Pharmacol 69:15–24
Pfreundschuh M, Trümper L, Kloess M, Schmits R, Feller AC, Rudolph C et al (2004a) Two-weekly or 3-weekly chop chemotherapy with our without etoposide for the treatment of elderly patients with aggressive lymphomas: results of the NHL-B2 trial of the DSHNHL. Blood 104:634–641
Pfreundschuh M, Trümper L, Kloess M, Schmits R, Feller AC, Rudolph C et al (2004b) Two-weekly or 3-weekly chop chemotherapy with our without etoposide for the treatment of young patients with good prognosis (normal LDH) aggressive lymphomas: results of the NHL-B1 trial of the DSHNHL. Blood 104:626–633
Price TH, Chatta GS, Dale DC (1996) Effect of recombinant granulocyte colony-stimulating factor on neutrophil kinetics in normal young and elderly humans. Blood 88:335–340
Pujo-Menjouet L, Bernard S, Mackey MC (2005) Long period oscillations in a G_0 model of hematopoietic stem cells. SIAM J Appl Dyn Syst 4:312–332
Quartino AL, Friberg LE, Karlsson MO (2012) A simultaneous analysis of the time-course of leukocytes and neutrophils following docetaxel administration using a semi-mechanisitic myelosuppression model. Invest New Drugs 30:833–845
Rankin SM (2010) The bone marrow: a site of neutrophil clearance. J Leukoc Biol 88:241–251
Riether C, Schürch CM, Ochsenbein AF (2015) Regulation of hematopoietic and leukemic stem cells by the immune system. Cell Death Differ 22:187–198
Rubinow S, Lebowitz J (1975) A mathematical model of neutrophil production and control in normal man. J Math Biol 1:187–225
Ryan DH (2016) Examination of blood cells. In: Kaushansky K, Lichtman MA, Prchal JT, Levi MM, Press OW, Burns LJ, Caligiuri M (eds) Williams Hematology, vol 9. McGraw-Hill Companies Inc., New York
Santillán M (2008) On the use of the Hill functions in mathematical models of gene regulatory networks. Math Model Nat Phenom 3:85–97
Sarkar CA, Lowenhaupt K, Wang PJ, Horan T, Lauffenburger DA (2003) Parsing the effects of binding, signaling, and trafficking on the mitogenic potencies of granulocyte colony-stimulating factor analogues. Biotechnol Prog 19:955–964
Schirm S, Engel C, Loeffler M, Scholz M (1996) Modelling chemotherapy effects on granulopoiesis. Br J Haematol 95:616–625
Schmitz S (1988) Ein mathematisches Modell der zyklischen Haemopoese. PhD thesis, Universitat Koln

Schmitz S, Franke H, Loeffler M, Wichmann HE, Diehl V (2014) Model analysis of the contrasting effects of GM-CSF and G-CSF treatment on peripheral blood neutrophils observed in three patients with childhood-onset cyclic neutropenia. BMC Syst Biol 8:1–18

Schmitz S, Loeffler M, Jones JB, Lange RD, Wichmann HE (1990) Synchrony of bone marrow proliferation and maturation as the origin of cyclic haemopoiesis. Cell Tissue Kinet 23:425–441

Scholz M, Engel C, Loeffler M (2005) Modelling human granulopoiesis under polychemotherapy with G-CSF support. J Math Biol 50:397–439

Scholz M, Schirm S, Wetzler M, Engel C, Loeffler M (2012) Pharmacokinetic and -dynamic modelling of G-CSF derivatives in humans. Theor Biol Med Model 9:1497–1502

Semerad CL, Liu F, Gregory AD, Stumpf K, Link DC (2002) G-CSF is an essential regulator of neutrophil trafficking from the bone marrow to the blood. Immunity 17:413–423

Shochat E, Rom-Kedar V, Segel LA (2007) G-CSF control of neutrophils dynamics in the blood. Bull Math Biol 69:2299–2338

Shvitra D, Laugalys R, Kolesov YS (1983) Mathematical modeling of the production of white blood cells. In: Marchuk G, Belykh LN (eds) Mathematical modeling in immunology and medicine. North-Holland, Amsterdam, pp 211–223

Smith CW (2016) Production, distribution, and fate of neutrophils. In: Kaushansky K, Lichtman MA, Prchal JT, Levi MM, Press OW, Burns LJ, Caligiuri M (eds) Williams hematology, vol 9. McGraw-Hill Companies Inc., New York

Spiekermann K, Roesler J, Emmendoerffer A, Elsner J, Welte K (1997) Functional features of neutrophils induced by G-CSF and GM-CSF treatment: differential effects and clinical implications. Leukemia 11:466–478

Terashi K, Oka M, Ohdo S, Furukubo T, Ikeda C, Fukuda M, Soda H, Higuchi S, Kohno S (1999) Close association between clearance of recombinant human granulocyte colony-stimulating factor (G-CSF) and G-CSF receptor on neutrophils in cancer patients. Antimicrob Agents Chemother 43:21–24

Vainas O, Ariad S, Amir O, Mermershtain W, Vainstein V, Kleiman M, Inbar O, Ben-Av R, Mukherjee A, Chan S, Agur Z (2012) Personalising docetaxel and G-CSF schedules in cancer patients by a clinically validated computational model. Br J Cancer 107:814–822

Vainstein V, Ginosar Y, Shoham M, Ranmar DO, Ianovski A, Agur Z (2005) The complex effect of granulocyte colony-stimulating factor on human granulopoiesis analyzed by a new physiologically-based mathematical model. J Theor Biol 235:311–327

van der Graaf P, Benson N (2011) Systems pharmacology: bridging systems biology and pharmacokinetics-pharmacodynamics (PKPD) in drug discovery and development. Pharm Res 28:1460–1464

von Schulthess GK, Mazer NA (1982) Cyclic neutropenia (CN): a clue to the control of granulopoiesis. Blood 59:27–37

Wang B, Ludden TM, Cheung EN, Schwab GG, Roskos LK (2001) Population pharmacokinetic-pharmacodynamic modeling of filgrastim (r-metHuG-CSF) in healthy volunteers. J Pharmacokinet Pharmacodyn 28:321–342

Ward AC, Monkhouse JL, Csar XF, Touw IP, Bello PB (1998) The Src-like tyrosine kinase Hck is activated by granulocyte colony-stimulating factor (G-CSF) and docks to the activated G-CSF receptor. Biochem Biophys Res Commun 251(1):117–123

Watari K, Asano S, Shirafuji N, Kodo H, Ozawa K, Takaku F, Kamachi S (1989) Serum granulocyte colony-stimulating factor levels in healthy volunteers and patients with various disorders as estimated by enzyme immunoassay. Blood 73(1):117–122

Wichmann HE, Loffler M (1988) Mathematical modeling of cell proliferation: stem cell regulation in hemopoiesis. CRC Press, Boca Raton

Wu X, Nekka F, Li J Steady-state volume of distribution of two compartmental models with simultaneous linear and saturated eliminations. Under review